# NOVEL PIEZOELECTRIC BIOSENSOR BASED ON SARS-COV-2 (COVID-19) SPIKE ANTIBODY FOR CORONAVIRUS (COVID-19) DETECTION

by

FARES SULAIMAN ALROMITHY

A dissertation submitted in partial fulfillment of the
requirements for the degree of

DOCTOR OF PHILOSOPHY IN ELECTRICAL AND COMPUTER ENGINEERING

2022

Oakland University
Rochester, Michigan

DOCTORAL ADVISORY COMMITTEE

Mohamed Zohdy, Ph.D., Chair
Gregory Auner, Ph.D.
Suzan Kamel-ElSayed, Ph.D.
Manohar Das, Ph.D.
Amanpreet Kaur, Ph.D.

بسم الله الرحمن الرحيم

محمد ﷺ

I dedicate this thesis to my mother, Maryam, my father, my lovely daughters, Maryam & Alma, my wife Randa, and my brother and sisters; without their love and guidance, it could never have been completed.

# ACKNOWLEDGMENTS

I cannot find words to express my gratitude to my advisors, Professor Mohamed A. Zohdy and Professor Gregory Auner, for everything they have provided me. Thank you so much for your guidance and encouragement, for sharing your expertise and advice, and for allowing me to take this research in its direction.

Thank you also to my committee members Professor Suzan Kamel-ElSayed, Professor Manohar Das, and Professor Amanpreet Kaur, for sparing your time to join this committee and for your comments and insights.

This thesis would not have been possible unless my mother, Maryam, My daughters, Maryam and Alma, and my wife, Randa. Thank you for your love, kindness, tenderness, guidance, patience, and everything you gave me.

I offer my regards and blessings to my brother Abdullah and my sweetheart, four sisters. Thank you for supporting me in any respect during the completion of this thesis.

Fares Sulaiman Alromithy

# ABSTRACT

NOVEL PIEZOELECTRIC BIOSENSOR BASED ON SARS-COV-2 (COVID-19) SPIKE ANTIBODY FOR CORONAVIRUS (COVID-19) DETECTION

by

FARES SULAIMAN ALROMITHY

Adviser: Mohamed Zohdy, Ph.D.

At the end of December 2019, the novel coronavirus SARS-CoV-2 appeared in Wuhan, China. The World Health Organization released a global health emergency declaration based on growing case notification rates in several locations worldwide. Therefore, sensitive, specific, rapid, and deliverable diagnostic monitoring is vital for making proper decisions on treating and isolating infected patients, which will help prevent the spread of infectious diseases. The surface Acoustic Wave (SAW) biosensor provides a unique, highly sensitive electrical approach to biomolecule detection and cell growth. For this study, a novel SAW sensor is developed, and the mass sensitivities are tested to detect the SARS-CoV-2 by attaching the SARS-CoV-2 spike antibody immobilized on the sensor surface. First, a two-dimensional (2D) and a three-dimensional (3D) finite element model were developed based on a realistic device to obtain a complete characterization of the senor. Then, the $AlN/Al_2O_3$ fabricated sensor was tested and ultrasonically rinsed in preparation for silanization. After depositions of (APTMS) on the sensor by the Chemical Vapor Deposition method, the antibodies were immobilized on surfaces with the aid of a crosslinker (EDC) and (Sulfo-NHS). Finally, the SARS-

CoV-2 was introduced to the sensor, and the attachment of the immobilized antibody was tested and evaluated. The sensor was tested and characterized by Raman spectroscopy and the vector Network Analyzer. Finally, our device was able to detect the virus in real-time time (within two to three minutes), confirming its high sensitivity and selectivity with regard to the SARS-CoV-2 virus.

TABLE OF CONTENTS

TABLE OF CONTENTS -Continued

TABLE OF CONTENTS -Continued

# LIST OF TABLES

LIST OF FIGURES

LIST OF FIGURES -Continued

# CHAPTER ONE

# INTRODUCTION

## 1.1 Problem Statement

At the end of December 2019, the novel SARS-CoV-2 (coronavirus disease 2019) appeared in Wuhan, China, and has spread into several other countries. In January 2020, The World Health Organization (WHO) released a global health emergency declaration based on growing case notification rates in several different locations around the world [1]. This SARS-CoV-2 virus is an extremely pathogenic zoonotic virus that has close genetic similarities to the Extreme Acute Respiratory Coronavirus (SARS-CoV) and the Middle East Respiratory Syndrome Coronavirus (MERS-CoV) [2]. Virus transmission may occur through coughing, aerosol particles, and close contact with inorganic materials and asymptomatic patients [3]. As a result of this pandemic, most scientific activities around the world continue to center on addressing this problem, first by improving ultra-rapid virus diagnosis and the isolation of infected people, and second, by identifying and developing effective vaccinations [3]. Consequently, the world faces a new challenge: developing ultra-fast, ultra-sensitive devices and nanoscale analytical instruments or sensing systems that are extremely efficient at detecting the COVID-19 virus.

The research community has been encouraged to perform a significant range of diagnostic studies to prevent the virus's propagation since monitoring is a critical method for evaluating the outbreak's epidemiology. Moreover, rapid diagnostic monitoring is vital for making proper decisions on treating and isolating infected patients, which will

help prevent the spread of infectious diseases [3]. The ideal diagnostic devices for a highly transmissible disease must have the ability to sense accurately, be affordable (e.g., low cost and low demand for staff and instruments), sensitive, specific (e.g., low rates of false positives and false negatives), rapid (e.g., preferably in minutes or within an hour), and the deliverable (e.g., accessible to the end-users) [4,5].

Although polymerase chain reactions (PCRs) are utilized for contemporary diagnostic procedures, they offer a sufficient detection level. Most laboratories can use mass spectrometry, but it might take longer to get the results to a laboratory specializing in mass spectrometry because of shipping delays. Even though fast lateral flow tests (both antigens and serological tests) are an excellent option for rapid point-of-care diagnostics, they have significant limitations. They do not always reach the sensitivity necessary for accurate diagnoses and monitoring. Therefore, developing next-generation diagnostic instruments that can overcome all of the constraints listed above and using piezoelectric biosensors are excellent choices for addressing such critical issues [6].

Biosensors are incredibly useful devices for use in the laboratory. These specialized devices, which combine a particular biological element and a transducer, provide high-sensitivity detection of a particular analyte in a wide range of biological samples. Coronaviruses, HIV, hepatitis B virus (HBV), hepatitis C virus (HCV), and Zika virus are among those that are detected using this method [7-13]. The antibody-antigen interaction is used in the creation of immunosensors. Generally, because of the highly specialized molecular interactions and affinity between an antibody and its antigen, they are more specific and sensitive than other biosensors. These molecules have affinity constants in the range of $10^8$ $M^{-1}$ and may reach as high as $10^{15}$ $M^{-1}$, which is

considerably greater than those of other biomolecules, such as enzymes, which typically have affinity constants in the region of $10^6$ $M^{-1}$. In combination with the extremely sensitive nature of piezoelectric (Pz) transducers, the specificity of this immuno-interaction produces an incredibly strong platform for sensor development [8]. Surface acoustic wave (SAW) biosensors have great sensitivity and operational robustness, and they have tremendous promise for integration into small smart devices that can be provided out of the lab at the point-of-care (POC).

## 1.2 Piezoelectric Biosensors for Detection of COVID-19

A biosensor is a device that detects the concentration of an analyte in a reaction by producing a signal proportional to the amount of the analyte present. Biosensors are used in the fields of disease detection, drug development, and environmental damage monitoring for use in blood, urine, saliva, and sweat [6]. The biosensors must be sensitive, accurate, reproducible, specific, nontoxic, and cost-effective. The many types of biosensors may be classified according to their fundamental principles of operation, including optical, piezoelectric, and electrochemical [7].

As shown in Figure 1.1 [6] the biosensors are essentially comprised of the following components:

- **Analyte**: The material of interest that must be detected. For example, glucose is used as an "analyte" in a biosensor intended to detect glucose level

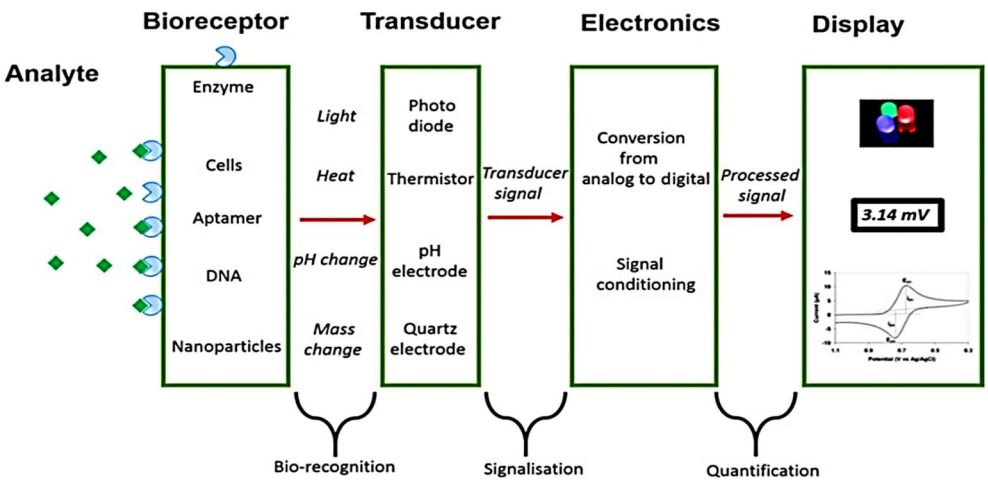


Figure 1. 1 Biosensor Components

- Bioreceptor: A bioreceptor is a molecule that identifies an analyte and only that analyte in particular. Bioreceptors include proteins, enzymes, cells, aptamers, deoxyribonucleic acid (DNA), and antibodies, to name a few. Bio-recognition is the process of signal production (in the form of light, heat, pH, charge, or mass change, among other things) that occurs due to the interaction of the bioreceptor with the analyte.

- **Transducer:** A transducer is a component that transforms one type of energy into another via conversion. The transducer is responsible for converting the bio-recognition event into a quantifiable signal in a biosensor. Signalization is the term used to describe this process of energy conversion. In most cases, optical or electrical signals are produced by transducers, and these signals are typically proportionate to the quantity of analyte–bioreceptor interactions that occurred.

- **Electronics**: This is the section of a biosensor that processes the signal that has

been transduced and prepares it to be displayed. Complex electrical circuitry is used to accomplish signal conditioning functions such as signal amplification and conversion of signals from analog to digital format. The biosensor's display unit quantifies the signals once they have been processed.

- **Display:** The display comprises a user interpretation system, such as a computer's liquid crystal display (LCD) or a direct printer that produces numbers or curves comprehensible to the user. This component is often composed of hardware and software that produces findings from the biosensor in a user-friendly format. The output signal on display may be numeric, visual, tabular, or a picture, depending on the end user's needs.

The biosensors can be classified into several categories, including optical, piezoelectric, and electrochemical sensors [9]. Optical transducers are the most basic sort of biosensor, and they may detect analytes or pathogens by measuring changes in the fluorescence, absorption, or reflectance properties of the sensing material [10]. This approach essentially takes advantage of the color change that occurs in the sensing materials when their size or concentration changes due to contact with the analyte or pathogen, which is simple and straightforward. The approach is based on the detection of changes in the resonance frequency of a biosensor, which is the second type of biosensor to be discussed here [11]. The electrochemical biosensor is the third type of biosensor, and it may be categorized into three types: Conductometric, Amperometer, and Potentiometric [12].

For the coronavirus disease 2019 (COVID-19) pandemic, Tianxing and Zhenwei et al. provided an overview of SARS-CoV-2 structure, genome, and gene expression features, as well as the current progress of SARS-CoV-2 ribonucleic acid (RNA), antibodies, antigens, and virus detection in relation to the pandemic [13]. The SARS-CoV-2 virus is mainly composed of an inner nucleic acid component that is coated by a spike glycoprotein on the surface. Cryo-electron microscopy has revealed the structure of a new coronavirus spike glycoprotein [12,13]. Eden Morales-Narváeza and Can Dincerb provided specific diagnostic approaches for identifying biomarkers associated with COVID-19 [8]. One of the most important targets was determined to be a variety of proteases and polymers [15]. It has been shown that SARS-CoV-2 enters host cells through the angiotensin-converting enzyme 2 (ACE2) receptor and that a protease inhibitor can prevent this entrance [14, 16,17]. It is possible to classify patients based on the severity of their condition by evaluating prognostic biomarkers and integrating this information with clinical observations and risk factors. In their study, Russell et al. proposed the ideal properties of the biosensors that may be considered a significant actor in precision medicine for COVID-19 [18].

Various antibody-based tests are being developed and tested for use in the detection and diagnosis of different pathogens [19]. The most frequently used procedures for diagnosing this condition are enzyme-linked immunosorbent assays (ELISAs) and polymerase chain reactions (PCRs) [20,21]. The viral surface spike protein and the device surface interact during the detection process. RT-PCR methods are extremely sensitive and specific, but they have expensive components, complex processes, and require a highly skilled operator [22, 23]. Furthermore, rapid mutations and false positive/negative

results have an impact on the effectiveness of these procedures [24]. However, due to the multistage analysis techniques, ELISA-based approaches require a longer assay time. In this regard, piezoelectric biosensors are the optimal devices since they provide label-free, real-time analysis with a sensitivity of up to the nanogram level [25, 26].

## 1.3 Objectives and Contributions

The SAW biosensor will be referred to throughout this dissertation as a device that was developed at Wayne State University as part of the Smart Sensors and Integrated Microsystems (SSIM) program. The sensor's core is formed via the deposition of a thin film of aluminum nitride (AlN) over a sapphire substrate ($Al_2O_3$). Aluminum nitride provides a variety of properties that make it a great material for biosensor operations. These advantages include high piezoelectricity, a high acoustic wave velocity, thermal stability, good lattice matching parameters to certain substrates, and linear thermal expansion with increasing temperature.

Throughout this dissertation, the concept of immobilization for biological detection is addressed. Since chemical and protein mediums must also be established for detection purposes throughout SAW biosensor fabrication, this portion of the process will be examined, and our approaches will be discussed in further detail. Additionally, this will be the first time, to our knowledge, that SARS-COV-2 (COVID-19) spike antibody immobilizations and SARS-CoV-2 virus detection on AlN grade plasma source molecular beam epitaxy (PSMBE) will be presented. The resonance frequency of our SAW biosensor is larger than 200 MHz. In addition, the substrate offers an environment in which covalent interactions can actually occur. Figure 1.3 illustrates the SAW biosensor's basic structure, including its main components.

For this study, the analyte of interest is SARS-CoV-2 (coronavirus disease 2019). The immobilizing agent must be bound to the sensor surface in order to immobilize the bioreceptor, which is SARS-CoV-2 (COVID-19) spike antibody. The two sets of interdigital transducers (IDTs) that are formed on the AlN surface transfer electrical signals into or out of the AIN layer. Acoustic waves propagate from one set of IDTs to the other across the sensing area when signals are transduced into and out of the AlN film. The spike antibodies were immobilized, and the changes in mass bound to the surface were detected in this sensing region.

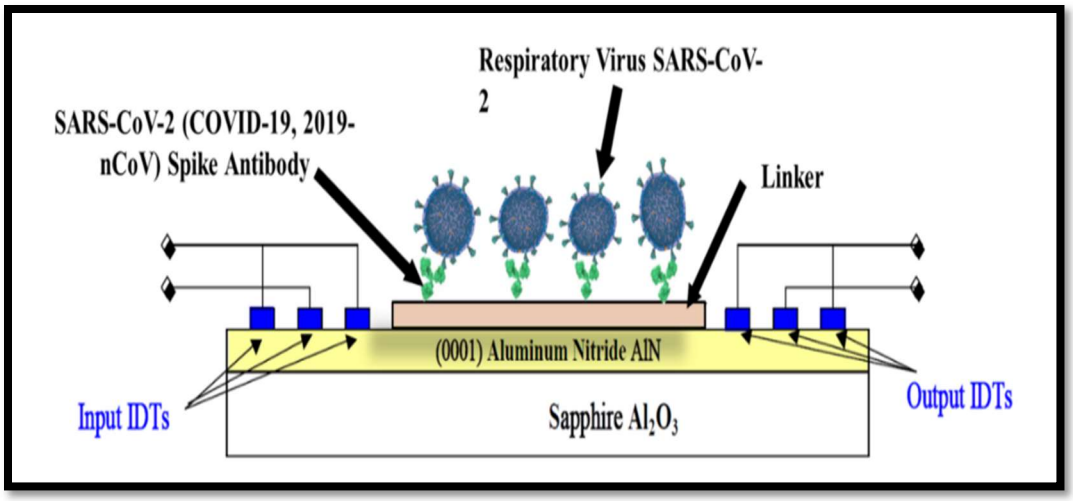


Figure 1. 2 The main Design of the SAW Biosensor

The unloaded AlN crystal film will oscillate at a certain resonance frequency when an electrical input signal is supplied at the beginning of the test. A shift in the resonance frequency will occur as a result of the mass being bound to the sensing area, and this frequency shift occurs in direct proportion to the increase in mass on the surface.

The frequency shift may be determined by comparing the input signal to the output signal of the sensing device. According to the sensor, the quantity of mass bonded to the surface is directly proportional to the frequency shift. Small variations in surface mass can theoretically be observed on the order of 10 ng/cm$^2$.

The following three objectives are a summary of the primary goals that this study aimed to accomplish with regard to immobilization of the spike antibody for purposes of SARS-CoV-2 detection:

**OBJECTIVE** 1: Development of functionalized Aluminum Nitride (AlN) surfaces for a novel shear horizontal surface acoustic wave SH-SAW biosensor (Design, Modeling, Fabrication, and Optimization).

**OBJECTIVE 2**: To immobilize the SARS-CoV-2 (COVID-19) spike antibody on the sensing region of the SH-SAW biosensor.

**OBJECTIVE 3:** Systematically characterize testbed a novel surface acoustic wave biosensor for immobilizing the SARS-CoV-2 spike antibody on the sensor surface and real-time detection of coronavirus 2 (COVID-19).

Therefore, in order to accomplish the crucial objectives of this study, there were four primary tasks that needed to be completed, and the following is a list of those tasks in the order of their level of significance:

- **TASK 1**: it was necessary to complete a series of theoretical derivation and analysis steps in order to ensure its overall quality. Finite element methods were examined and implemented with the COMSOL Multiphysics® software to obtain the quantitative analysis. Three- and two-dimensional FEM simulations were successfully performed.

- **TASK 2**: The task mission to prepare the SH-SAW biosensor, which was fabricated in our SSIM clean room by tested, calibrated, and optimized by using the Chemical Vapor Deposition (CVD) method for deposition of a 3-Aminopropyltrimethoxysilane (APTMS) as a chemical linker layer that would enable the immobilization of spike antibody on the device surface. The optimized device was measured and tested with the use of a vector network analyzer, and the results were compared with the verification results obtained from COMSOL simulation models.

- **TASK 3**: the heterobifunctional crosslinkers 1-Ethyl-3-(3 dimethylaminopropyl)-carbodiimide (EDC) and sulfo-N-hydroxysuccinimide (Sulfo-NHS) were utilized in order to immobilize covalently bound proteins on APTMS functionalized AlN surfaces in preparation for covalent spike antibody immobilization. Raman microscopy was conducted in order to confirm that antibodies had been successfully immobilized onto amino-silanized AlN surfaces.

- **TASK 4:** The main goal of this task is to test and investigate the selectivity and sensitivity of the fabricated SH-SAW biosensor for SARS-CoV-2 detection in real-time. Human coronavirus OC43, Influenza B Yamagata, and SARS-CoV-2 viruses were each introduced to the device sensing area at a varied volume and concentration.

Finally, the main goals and objectives of this work have been achieved, and the SARS-CoV-2 (COVID-19) spike antibody was successfully immobilized on the $AlN/Al_2O_3$ biosensor, and the result was achieved and confirmed using the Raman Spectroscopy. In addition, systematically characterized and testbed a novel surface acoustic wave biosensor for immobilizing the SARS-CoV-2 spike antibody on the sensor

surface and real-time detection of coronavirus 2 (COVID-19), the virus was detected by our device in real-time (2-3 minutes) with the confirmation high sensitivity and selectivity regarding the SARS-CoV-2 virus. Figure 1.3 summarize task 1 and task 2; also, Figure 1.4 summarize task 3 and task 4.

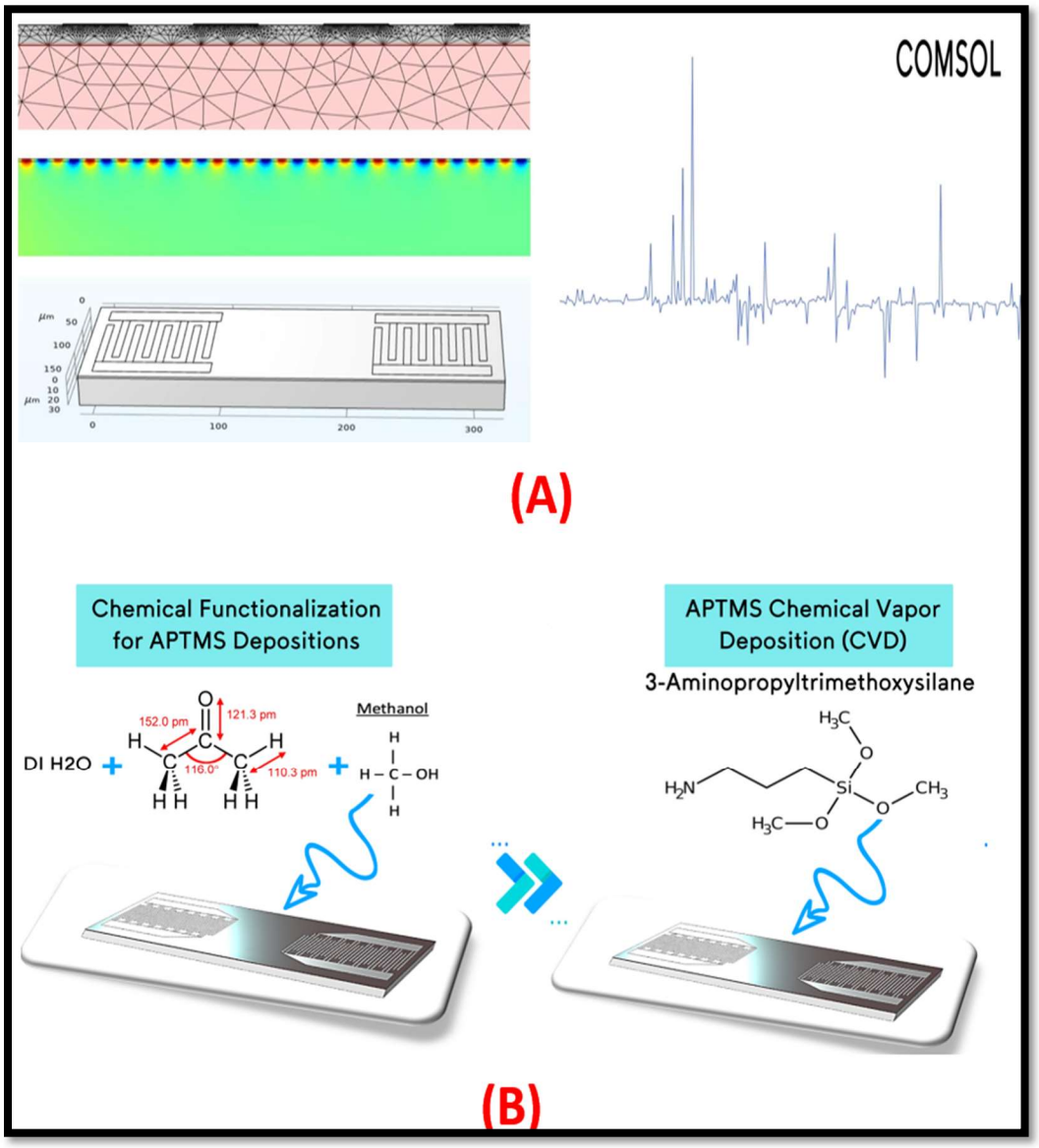


Figure 1. 3 (A) Summarize Task 1, (B) Summarize Task 2

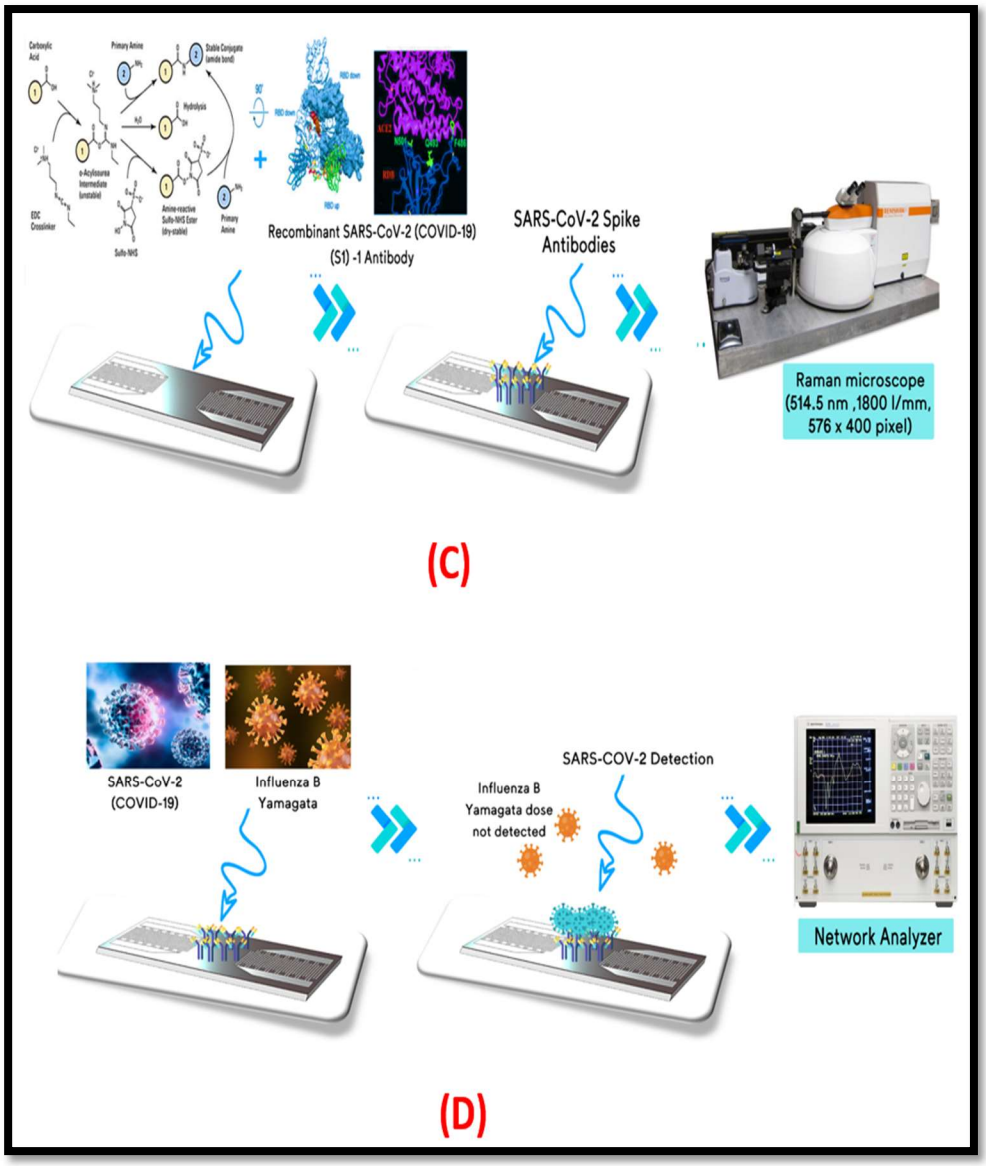


Figure 1. 4 (C) Summarize Task 3, (D) Summarize Task 4

# CHAPTER TWO

# LITERATURE REVIEW

In recent years, newly emerging viral illnesses have risen to the level of a significant public health threat in many places around the world. Several viral infections have been reported in outbreaks during the last two decades, including the severe acute respiratory syndrome coronavirus (SARS-CoV) in 2002, H1N1 influenza in 2009, the Middle East respiratory syndrome coronavirus (MERS-CoV) in 2012, Ebola virus disease (EVD) in 2013, and the Zika virus in 2015 [27-32].

Since January 2020, a severe acute respiratory syndrome coronavirus (SARS-CoV-2) outbreak has spread worldwide, resulting in a global pandemic. Researchers from a wide range of disciplinary backgrounds have investigated various aspects of the pandemic outbreak. The current situation has illustrated how the steady development of nanotechnology and nanoscience can aid in the enhancement of defenses against deadly viruses in the future. Current and future pandemic outbreaks will require the development of diagnostic techniques that can rapidly identify infected individuals, as well as disease transmission, in order to control the spread of the virus and reduce the risks.

In previous published studies, various approaches have been developed for the specific detection of the virus, all of which are based on identifying the viral nucleic acids during acute infection [27-32]. These techniques are described in detail below. However, as the prevalence of SARS-CoV-2 infection increases around the world, there is a greater requirement for early diagnosis in both symptomatic and non-symptomatic cases, as well as better analysis.

The most important technique in the defense against virus spread is slowing its transmission rate, which may be accomplished in part by closely monitoring affected persons and their connections. SARS-CoV-2 discovery in an organism is the first step toward achieving effective control of the disease. As a result, the development and implementation of rapid, specific, and sensitive detection technologies are necessary. The structure of SARS-CoV-2, its life cycle, and the induced host response should be discussed in more depth to get a better understanding of the concepts behind the present detection methods.

## 2.1 Overview of SARS-CoV-2

Coronaviruses (CoVs) are enveloped, positive-sensed, single-stranded ribonucleic acid (RNA) genome viruses that belong to the Coronaviridae family. The unique feature of a positive-sense RNA genome is its ability to be directly employed for translation of the nucleic acid molecule, resulting in the production of multiple copies of protein molecules. CoVs are divided into four genera (alpha-CoV, beta-CoV, gamma-CoV, and delta-CoV) based on protein sequence differences, including the beta-CoV genera containing the majority of human CoVs (HCoVs) [33].

According to phylogenetic evidence, bats and rodents are the gene sources for most alpha- and beta-CoVs, while birds are the main reservoir for gamma- and delta-CoV. Only seven humans CoVs (HCoVs) have been identified to date, two of which are alpha-CoVs (HCoV-229E and HCoV-NL63) [33,34].

In addition, the other five beta-CoVs contain HCoV-OC43, HCoV-HKU1, severe acute respiratory syndrome coronavirus (SARS-CoV), Middle East respiratory syndrome coronavirus (MERS-CoV), and SARS-CoV-2 [33,34].

As shown in Figure 2.1 [35], SARS-CoV-2 is a spherical, encapsulated virus with surface projections that give the virus its corona appearance [35]. With an average diameter of 80–90 nanometers, the virus is mainly composed of a single-stranded positive-sense RNA (+ssRNA) particle [36]. This strain of SARS-CoV-2 virus has a total genome of 29891nucleotide, 9860 amino acids, and length ranging from 26 to 32 kb (kilobases) [37, 38].

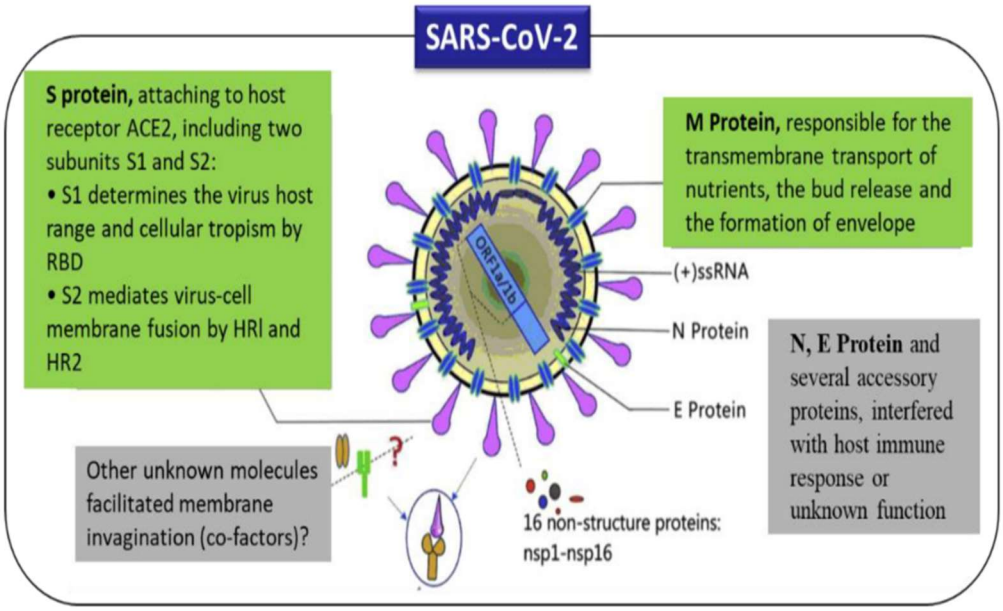


Figure 2. 1 SARS-COV-2 Structure and Main Proteins

There are 29 proteins in the SARS-CoV-2 genome, four of which are structural proteins and one of which is an RNA-dependent polymerase (RdRP). At the 5′ end of the genome, there are two open reading frames (ORFs) labeled ORF1a and ORF1b, while a third section at the 3′ end of the genome contains genes responsible for structural and

accessory proteins [36]**.** Additionally, it contains four critical structural proteins: the spike glycoprotein (S protein), which has a molecular weight of around 141000 kDa, the envelope protein (E protein, which has a molecular weight of 8–12 kDa), the membrane protein (M protein), and the nucleocapsid protein (N protein) [38,39]**.**

In the entrance of SARS-CoV-2 into the host, one of the most critical proteins is the SARS-CoV-2 spike glycoprotein, which contains both the receptor-binding domain (RBD) and the fusion domains [34]. The spike glycoprotein is 1273 amino acids in length and is described as a trimeric protein with three domains (S1, S2, and S2`). Spike S1 and Spike S2 proteins are involved in cell membrane attachment/binding and fusion [13,40, 41]. It was discovered that the SARS-CoV-2 spike protein's hydrophobic phenylalanine residue was responsible for the protein's strong interaction with the angiotensin-converting enzyme 2, ACE2 [42]. This demonstrated that hydrophobic and electrostatic interactions are critical for SARS-CoV-2 attachment/binding [41]. The core sequence of spike S1 protein was analyzed and found to have 46% hydrophobic, 36% hydrophilic, 10% positively charged, and 8 % negatively charged residues [41]. As a result, it is anticipated that a significant interaction between the spike S1 protein and hydrophobic and negatively charged surfaces would be observed [41].

A protease enzyme called TMPRSS2 is responsible for the virus's initial attachment to the host cell and subsequent entry into it. SARS-CoV-2 enters host cells via the binding of S glycoprotein to the host cell receptor, since this protein aids in the merging of the host cell and viral membranes. This allows the SARS-CoV-2 virus to enter the host cell more easily [34,39], where viral RNA immediately converts into proteins, accompanied by RNA synthesis via virus replication in the cytoplasm [38]. Both

the spike protein and the host cell receptor are directly associated with amino acid sequence variations [43].

In order to acquire entrance into a host cell, the virus uses the S protein to attach to angiotensin-converting enzyme 2 (ACE2) on the cell surface [44]. For diagnosis of SARS-CoV-2, genes such as ORF1ab, the RNA-dependent polymerase gene, the E protein, and the N protein can be targeted for diagnosis [36]. Otherwise, antibodies like IgM and IgG from patient samples could also be detectable [44]. Numerous studies demonstrate that IgM antibodies become detectable about 5–10 days after the onset of symptoms and rapidly increase, shortly followed by an IgG antibody response [44]. As a result of these viral infections and immune response investigations, the detection window for SARS-CoV-2 diagnosis is clearly defined, as well as a strategy for implementing appropriate tests at various stages of infection.

### 2.2 Diagnostic Strategies for SARS-CoV-2 Detection.

Early detection of emerging pathogens is critical for clinical point of care (POC) environments. Biological labels such as radioisotopes, enzymes, and fluorophores can be detected in medical diagnostic laboratories using a variety of analytical techniques, including polymerized chain reaction (PCR) amplification and enzyme-linked immunosorbent assays (ELISA). Although these techniques are particularly sensitive and selective, multiple detection layers are typically used to detect various analyses. The demand for highly qualified staff, lengthy analysis timeframes, and significant effort and resource costs frequently have a negative impact on diagnosis. Therefore, there is a critical need for effective

virus detection devices that are easy to operate, have rapid response times, high selectivity, cross-sensitivity, and portability.

### 2.2.1 Clinical and Laboratory Testing

Immunological assays and amplification techniques are two types of clinical detection methodologies that can be used to detect SARS-CoV-2 viruses in the clinic and laboratory. In order to diagnose SARS-CoV-2 viruses, various types of diagnostic tests are being employed, including chest computed tomography (CT) scan along with clinical symptoms, RNA detection using real-time reverse transcriptase-polymerase chain reaction (RT-qPCR) assay, and Lateral flow immunochromato-graphic strip (LFICS), fully automatic chemiluminescence assay and enzyme-linked immunosorbent assay (ELISA) based antibody detection [45, 46].

Regarding the chest computed tomography (CT) scan procedure, X-ray image of the chest is combined with computer processing to create cross-sectional images (slices) of the lung [47]. A diagnostic criterion for SARS-CoV-2 has been established based on its radiologic characteristics [49, 51]. Recently, a 3D deep learning framework based on chest CT images was developed for the diagnosis of SARS-CoV-2. The model tested had a sensitivity of 90% and a specificity of 96%, according to the results [50]. However, a CT scan is a diagnostic procedure that requires specialized training and expensive medical instruments that is only available in a few select central hospitals.

The real-time reverse transcription-polymerase chain reaction (rRT-PCR) is routinely used to detect viruses and has been widely used by the Center for

Disease Control and Prevention and other relevant departments worldwide and provides accurate results [52]. Detection efficiency and accuracy are strongly linked to the quality of the specimens. Research is being conducted on samples from the upper and lower respiratory tracts, including samples taken from the mouth and nose, as well as swabs from the throat and deep-throat saliva. Samples from the lower respiratory tract have a lower false-negative rate when using RT-qPCR to detect RNA [47]. The nasal specimen shows a greater viral load than the throat specimen for upper respiratory tract specimens [52]. On the other hand, the RT-PCR assay can take up to four hours to complete one test and is highly susceptible to generating false-negative results in a significant proportion of cases studied [45]. It is also possible that additional proteins present in serological samples are responsible for the false-positive results [47].

Therefore, there is an important and urgent need for the development of low-cost, high-performance point-of-care (PoC) devices that can deliver reliable, rapid, and robust responses. The tools that are designed for this purpose should be simple enough to be utilized on-site and in the field without the need for specially trained personnel to operate them.

### 2.2.2 Biosensors for Coronavirus Detection

Biosensors use the binding of nanoparticles to target molecules of interest to generate a quantifiable signal, allowing the detection of biomarkers or pathogens [54] [55]. In biosensors, nanotechnology methods are used, and the operations are carried out at a nanoscale, resulting in hand-held devices that are easy to use and marketable, as well as robust, highly sensitive, and reliable. As a result of this, early detection of diseases and

the ability to do rapid testing are significant advantages. Antibodies, enzymes, nucleic acids, microorganisms, cells, tissues, and even some biomimetic structures are commonly realized in the biological recognition component of biosensors [56, 55]. Additionally, when demand grows for biosensors, all constituents can be designed and fabricated in appreciable amounts at a reasonable cost to meet customer requirements.

Figure 2.2 [54] illustrates the various types of biosensors provided for SARS-CoV-1 and MERS-CoV detections [55]. It is possible to classify the devices according to the biological molecule (nucleic acids, antigens, or antibodies) that has been immobilized on the sensor surface. The particular interaction involving immobilized probes and specific targets results in a physicochemical change that can be converted into a quantifiable signal for detection by using a signal processor.

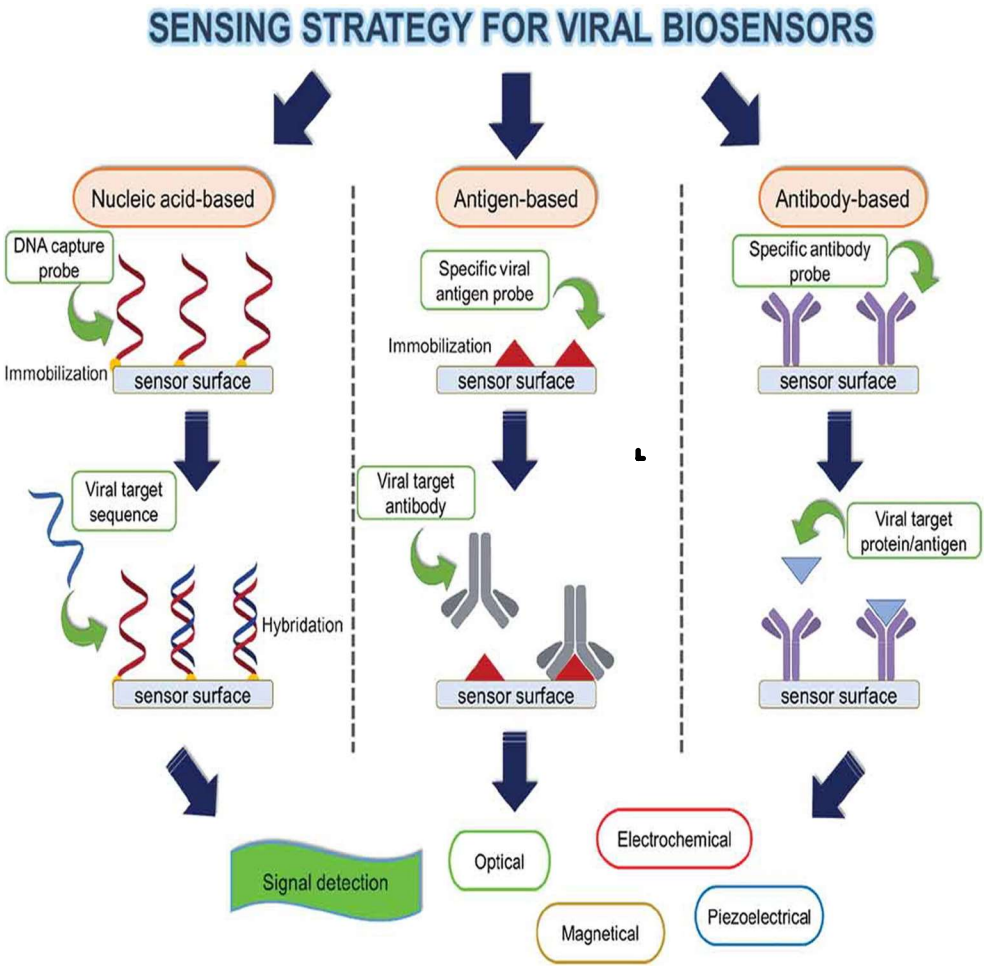


Figure 2. 2 The different types of biosensors characterized for SARS-CoV and MERS-CoV

2.2.2.1 Single-stranded RNA-Based Biosensor

With a length of around 30 kilobases and an amino acid sequence of 9760 amino acids, the positive-sense single-stranded RNA genome of SARS-CoV-2 serves as a critical biomarker for the detection of the virus.[47,54]. Generally, genes that are conserved or that are fully expressed are the most desirable targets for RT-PCR tests [46, 48]. SARS-CoV-2 can be detected with great sensitivity using special primers that specifically target these genes while simultaneously

ruling out the detection of other comparable types of viruses such as the Middle East respiratory syndrome (MERS) and influenza [49]. Assays targeting the N and S genes of SARS-CoV-2 were developed, with three different varieties being compared to one other. The assays targeted the N and S genes of SARS-CoV-2 and were constructed using remarkable RT-PCR technology [50]. The great sensitivity will be achieved by using nasopharyngeal samples, and there will be no cross-reactivity with other coronaviruses observed during the process [47].

2.2.2.2 Whole Virus and Antigen-Based Biosensor

SARS-CoV-2 contains a total of 28 unique protein types [51] . The structural proteins S, M, E, and N proteins could be used as antigens in the diagnosis of SARS-CoV-2. M and E proteins have a crucial part in the development of the viral structure, according to various studies [27]. The S protein is extremely important because it forms interactions with host cells, and the receptor-binding domain of the S protein interacts with ACE2 receptors, which are present in many regions. Because the same proteins have been utilized in various ways for the detection of SARS-CoV in the past, it is more likely that S and N proteins will serve as important antigen biomarkers that will be used for the detection of SARS-CoV-2 [52]. Jiang et al. recently developed a proteome microarray that included 18 of 28 proteins and used it to evaluate antibody responses [53]. Patients in the recovery stage have a significant antibody response to the proteome, particularly to protein N and S1, but not to protein S2. Furthermore, the use of lateral flow assays for the diagnosis of SARS-CoV-2 has

allowed researchers to investigate a viral protein-based detection technique for the virus.

2.2.2.3 Antibody-Based Biosensor

The diagnosis of SARS-CoV-2 can also be made through the detection of specific antibodies to the virus in serological samples collected from patients with the infection. It is generally indicated that IgM responses occur early onset of a viral infection, whereas IgG responses take place late in the period of the infection or during long-term immunity [54]. According to the findings of a study conducted by Zhang et al., the detection of IgM and IgG antibodies in patients could be performed within five days of the onset of symptoms [55]. According to the results of another study, which focused on the detection of IgM and IgG in nucleic confirmed patients, different percentages of antibodies were observed at different stages of SARS-CoV-2 infection. For example, 11.1 percent of antibodies were found at the early stage up to the 7th day, 92.9 percent at the medium stage up to the 14th day, and 96.8 percent at the later stage after the 15th day of onset of symptoms [56]. Until this point, the diagnosis of SARS-CoV-2 with anti-bodies detection assays has proven to be insufficiently effective. The detection of antibodies can be beneficial to patients during the recovery phase, and it is extremely important for the design of vaccines because the exact quantity of antibodies detected correlates with virus neutralization titer [54].

## 2.3 Surface Acoustic Waves in Biosensing Applications

### 2.3.1 Overview

A biosensor is an analytical device capable of detecting the presence of a biological analyte using a bioreceptor and a physiochemical transducer. Biological analytes include biochemistry structures, biomolecules, or macromolecules [6,57]. The output data of a biosensor is a measurable signal resulting from an energy conversion of the bio-recognition event [6]. Biosensors are designed for a multitude of recognition elements, which include cell organelles, antigens, enzymes, microorganisms, nucleic acids, antibodies, tissues, receptors, and whole cells [6]. Every biosensor possesses some attributes; however, selectivity is a significant feature of an effective biosensor for detecting an analyte in the presence of other admixtures [58].

Moreover, a biosensor's sensitivity is another feature that is significant for detecting and measuring an analyte concentration in a sample for the sake of disease diagnosis and monitoring [57,59]. With the advances in modern technology, the enhancement of effective biosensors elicits goals such as developing low-cost biosensors, the ability of using minimal pre-treatment of the sample and small volume samples, and using minimal technical skills [60]. Furthermore, to achieve these goals and build sensitive and selective miniaturized, inexpensive point of care (POC) biosensors, short incubation time and biofouling from the accumulation of non-specifically bound proteins are some of the important issues that must be tackled and solved [60,61].

### 2.3.2 SAW sensor in Biosensing

In the field of sensing and material characterization, acoustic waves have proved to be significant in the manufacture of sensing devices. Mainly, there are four acoustic wave devices that include thickness-shear mode (TSM) resonators, acoustic plate mode (APM), surface acoustic wave (SAW), and flexural plate wave (FPW) devices [5, 22, 60,62,63]. These acoustic wave devices are either one-port or two-port devices. The one-port devices such as the TSM resonators possess one port for both the input and output, where the input signal creates a propagated acoustic wave that produces electrical charges on the input port. However, the two-port devices such as SAW, APM, and FPW devices possess an input port and another output port, where an acoustic wave is produced from the input signal, and its propagation is transferred by a transducer to the outport port as an electrical signal [58 – 61].

According to a previous study [64], the SAW biosensors were found to be effective for POC biological testing applications. Considering that SAW biosensors are highly sensitive, they are capable of detecting and removing non-specifically bound protein, interfering with the sensor signal, and decreasing incubation times in a way to build compact and selective POC biosensing systems to perform effective medical diagnostics. Moreover, the potential of acoustic streaming generated from SAW to remove NSB protein and mix components can be exploited to enhance the biosensing platforms by blending them with other analyte quantification modalities such as fluorescence and electrochemical ones [64]. Low-cost compact SAW biosensors allow the

quantification of biomarkers at POC from liquids such as blood and urine. Real-time detection of antibodies to hepatitis B surface antigen (HBsAg) was also accomplished through the use of the SAW immunosensor device [65]. HBsAb was detected in real blood samples using the device that was successfully developed.

Vapor and biomolecule detection can be carried out using SAW biosensors by noticing frequency shifts based on the effect of tiny mass loading of analytes. Mass loading has the ability to adjust and tune frequency shift to picogram level using the SAW surface [66]. Notably, connecting biomolecules to the surface can assist in achieving reproducibility and stability of bioreceptors.

For instance, when providing three layers of different odorant binding proteins (OBPs) to a system of five SAW bioreceptors, it would be convenient to detect and measure the concentrations of octenol and carvone vapors using the corresponding shifts in resonant frequency [67]. Another example is the fruit ripeness system that was created as a sensitive coating from zinc oxide, and with the lithium niobate-based gas sensor, it was possible to detect the concentration of ethylene, which can determine the various ripeness levels of fruits [68]. In the field of SAW-based gas sensors, more research is required to enhance substrate stability, find electrode materials that can endure severe sensing environments, and utilize highly developed sensing materials and numerous SAW resonator arrays to detect and quantify complex gases [69].

Occasionally, the detection of intercellular macromolecules such as proteins that can detect pathogens, DNA, and RNA through the use of sensing applications requires disruption or lysis of cell membranes. Due to the growing

need for miniaturized lysis systems, SAW provides a powerful approach for the development of these systems. Basically, cell lysis has been achieved through the use of ultrasound depending on bulky high-power equipment and fairly large volume sample [70]. In addition, bulk acoustic wave (BAW) devices were used in a way to decrease sample size and power consumption. However, the SAW uses a smaller sample volume, and its property of surface trapping of acoustic wave energy makes it more effective than BAWs [70]. Furthermore, in a study for detecting pancreatic cancer, SAW was used to cause lysing of exosomes for RNA detection [71]. In this study, twenty pairs of titanium/aluminum interdigitated electrodes (IDTs) were modeled on a 127.68° YX-cut piezoelectric lithium niobate ($LiNbO_3$) substrate to create SAWs that propagate in one direction, and the operating frequency was found to be 28.3 MHz. The cell lysis using SAW was performed by introducing the sample to 30 s of SAW at 1W power leading to the production of a lysis rate of 38% that enabled exosome RNA detection and identification [72].

Another application of SAW in biosensing is the monitoring of cell adhesion which delivers significant data about the function of the cell regarding the formation of body tissues and many other medical problems such as bone repair [73]. Cell adhesion can be determined by detecting and measuring the binding affinity of proteins located on the surface of a cell [74]. The SAW method allows carrying out kinetic evaluations by detecting the binding kinetics at the sensor surface that leads to alternations in the wave phase and amplitude, equilibrium dissociation, and conformation changes [75]. While the changes in

the phase of the wave are associated with mass loading, the changes in amplitude are a result of the variations in the viscosity of the bound molecules [76].

### 2.3.3 SAW immunosensors

The performance of immunosensors is established by means of the specific interaction and binding of antibodies and antigens [60]. The antibody or the antigen that needs to be detected will be dissolved in the solution prepared for testing, while the other will be bound to the surface of the sensor in a way to determine changes in mass due to the binding reaction. Immunosensors are considerably used to detect and measure a variety of antigens [60]. The first study used to detect an antigen using SAW devices and deactivated antibody was conducted by Roerder and Bastians [77]. ST-X Quartz was the material used for the sensing device that was settled in an oscillator circuit. This device was used for detecting shifts in frequencies, which relate to the quantity of antigens bound to the surface. While this device was able to detect and measure human IgG, it failed to detect small molecules due to its low sensitivity. More advancements were made to improve this device, and Welsch and colleagues were able to utilize the first immunosensor that used SH-SAWs on a LiTaO3 substrate [78].

Devices that generate surface acoustic waves employ a piezoelectric substrate, which produces waves when an electrical electric field is applied. Acoustic devices are therefore responsive to species physical factors that interact with mechanical features of guided waves in the SAW sensors. This means that SAW sensors used for chemical or biological detection are built such that the transducer layer may interact with these

substances. A particular mechanical or electrical response is then transmitted as the result of these interactions [80-87].

Equation (2.1) [88] elucidates, in a linear sense, the interruption of the acoustic wave velocity that is caused by mass, electrical characteristics, mechanical qualities, and environmental factors. The velocity of the SAW in the substrate, denoted by the letter V, is a function of a number of different physical and environmental conditions. An object's velocity (v) is determined by its mass, as well as the effects of its electrical and mechanical characteristics, as well as the environment, which might include factors like temperature, humidity, and pressure. This could be represented as ($\partial$V) by employing the chain rule in the case where V is the wave velocity change, as shown in Equation 2.1:

$$dv = \frac{\partial V}{\partial m} dm + \frac{\partial V}{\partial E} dE + \frac{\partial V}{\partial M_i} dM_i + \frac{\partial V}{\partial e_v} de_v \tag{2.1}$$

where the velocity is a function of the mass, which is defined by m; the effect of the electrical properties, which is indicated by E; the influence of the mechanical properties, which is denoted by $M_i$; and the effect of the environment, which is represented by $e_v$.

SAW sensing parameters can be generically categorized into a few parameters such as mass, density, viscosity, elastic modulus, conductivity, temperature, and pressure. The wave velocity change would not be able to differentiate between the numerous changes in Equation (3.1). However, change in wave velocity (dv) isn't the only way to monitor influence parameters or sensing variables using SAW sensors. A complete time history signal from an IDT receptor might be collected if a SAW sensor is used. Wave signals received by receptor end IDTs can be studied further. Wave signals carry numerous signal properties that may be altered by individual sensing variables yet look

coupled while measuring (dv). As a result, in order to evaluate nonlinearity, it is necessary to detect the change in amplitude of the core frequency, the frequency shift of the given frequency input, the phase change, and higher-order frequency peaks.

Sensitivity is defined as the ability of sensors to detect even the smallest of changes in the parameters they monitor. The major analytes are used to determine the sensitivity of detection, not the other parameters individually. It is possible for a SAW sensor that was built expressly to monitor changes in temperature to have a high sensitivity while at the same time having a very low sensitivity when it comes to measuring the mass loading. Because of this, it is not guaranteed that SAW sensors will have a high sensitivity for all additional parameters.

Geometric configuration and specific material, as well as a specific design of IDTs, are required for an application-driven SAW sensor to ensure that a certain mechanism can be detected via an additional secondary parameter. Antigen (Ag) can bind to a specific antibody, and it is possible to accomplish their chemical and biological reaction by using a SAW sensor. The wave velocity and/or frequency amplitude may be affected by this reaction in mass loading. So, the sensitivity can therefore be described as the ability to detect a small amount of Ab. For the most part, a feature identifies the primary process by pointing to the change in secondary parameters as an observable [88].

Selectivity, on the other hand, describes how precise detection can be. Mass loading will not be affected by a different antibody (Ab) that does not bind to an antigen (Ag), and the detection should be negative. Negative detection should only occur when another Ab is present, which means that positive detection is only possible when the Ab is present. When using SAW sensors, it is not unusual to get both false positives and false

negatives. Both of these scenarios reduce the sensors' sensitivity and selectivity. Selectivity is not a guarantee of a highly sensitive sensor, even if it is proved. Similarly, if a sensor's sensitivity is increased, it is not guaranteed to be extremely selective. Thus, multi-channel and multi-aperture detection is required in SAW sensors in order to concurrently ensure sensitivity and selectivity. The sensitivity and selectivity of sensors can be improved by adding more fingers to IDTs and using more than one IDT terminal. As a result, ultrasonic frequencies are used in SAW devices, and an ultrasonic wave travels through the substrate.

## 2.4 Antibody and Chemical Binding Strategies for SAW Biosensors

### 2.4.1 Introduction to Antibody

Antibodies are serum glycoproteins that are extremely soluble and are involved in the immune system's defense mechanisms [89]. An important factor in biosensor performance is the orientation of surface-immobilized capture proteins, such as antibodies [90]. The characteristics of the biorecognition elements utilized for analyte binding determine the biosensor's sensitivity and selectivity [91]. Antibody presentation affects the sensitivity of immunodiagnostic processes, with optimal performance demanding that the antigen binding sites be directed toward the solution phase [90]. An efficient technique for the detection of a diverse range of analytes from the category of antigens and haptens is the use of immunosensors that employ antibodies as binding proteins [91]. Genetic engineering provides an elegant method not only for the synthesis of essentially endless quantities of biorecognition molecules but also for the change of existing features and the addition of new functionalities to biorecognition molecules that have already been discovered [91]. A set of B cells were used to create an antibody

library, and the improved binders were produced by rearranging the heavy and light chains of the antibody [91].

Antibodies can be divided into five classes depending on their heavy chain constant region sequences, i.e., IgM, IgD, IgG, IgE, and IgA [89]. Antibodies are biopolymers of approximately 150 kDa molecular mass and with dimensions of approximately (14 x 10 x 4 nano meters) they consist of four polypeptide chains, i.e., Y-shaped molecules are formed by the combination of two light chains and two heavy chains held together by disulfide bonds [90] [92]. Like any other protein, chemically, an antibody possesses carboxyl, amine, hydroxyl, sulfhydryl, alkyl, and aryl functional groups [93].

As shown in Figure 2.3 [93], the basic structure of an antibody can be subdivided into two distinct building blocks: fragment antigen binding (Fab) regions and a fragment

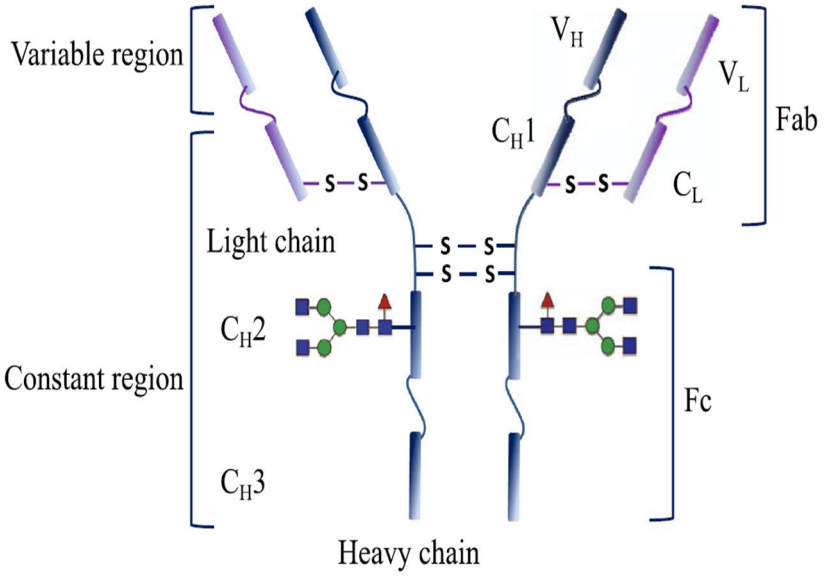


Figure 2. 3 Schematic Representation of an Antibody Molecule

crystallizable region (Fc) [89] . The heavy chain consists of one variable region ($V_H$) that is responsible for antigen binding and three constant regions ($C_H1$, $C_H2$, and $C_H3$).

There is one variable area in the light chain ($V_L$), which is an important part of the antigen-binding site, and one constant region (CL) [89]. The variable domain contains three hypervariable regions that are referred to as complementarity-determining regions (CDRs). These regions are responsible for the specific interaction between the antibody and the antigen [92] . The endless supply of Abs with varying degrees of septicity and binding strength (affinity) is made possible by the diversity that exists in this area [92].

### 2.4.2 Overview of Antibodies Formats

The availability of antibodies in such a wide variety of forms contributes significantly to the adaptability of these molecules. Researchers and medical professionals have access to a wide range of species from which they can select monoclonal or polyclonal antibodies to use in their studies. The antibodies can be utilized either as whole molecules or as any one of numerous different forms of fragments. Furthermore, the antibodies can be chemically attached to a wide variety of different kinds of reporter molecules. Due to the obvious availability of these capabilities, antibodies may be tested using an even greater variety of different types of platforms [69].

Antibodies have been used extensively since their initial discovery as diagnostic tools in many different formats due to their exquisite specificity for their associated antigen [89], [92], [94]. Conventional techniques for the preparation of Ab in antiserum against a specific target consistently result in the production of non-homogeneous Abs with different specificity and affinity, referred to as polyclonal Ab (pAbs) [89].

Monoclonal Ab (mAb) technology or hybridoma technology has revolutionized the use of Ab as a research tool for the prevention, detection, and treatment of diseases [89], [94]. Many monoclonal and polyclonal antibodies are commercially accessible, and they are derived from a diverse range of mammalian species, including humans (e.g., goats, rabbits, mice, etc.). Polyclonal antibodies are derived from multiple plasma cells, and monoclonal antibodies are derived from a single clonal hybridoma, all of which have terminally differentiated in response to an antigen [94].

Traditional IgG monoclonal antibodies (mAbs) have a place in the diagnosis and treatment of diseases; however, the development of recombinant antibody (rAb) technology and a greater comprehension of antibody research have opened the door to innovative and vastly superior strategies for a generation of antibodies to emerge which can be used in diagnostics as well as treatment. The technique of recombinant antibodies enables the creation of antibody fragments that maintain their integrity and sensitivity. These minimized antibodies have several advantages over their parental counterparts, namely in clinical practice. These advantages include better tumor penetration, more rapid blood clearance, lower retention times in non-target tissue, and reduced immunogenicity compared to the primary parental antibodies [89].

Recombinant antibodies are the product of the genetic manipulation of antibody genes [94]. The key parameters that exist for antibodies in biosensor applications include sensitivity, selectivity, stability, immobilization (hence, orientation on the surface), labeling, and antibody size (i.e., impacts on the density of the sensor's biolayer) [94]. Recombinant antibodies present a viable means to optimize these factors [94]. Primarily genetic modification facilitates improvements in selectivity, stability, and size [89].

### 2.4.3 Antibody Immobilization General Approaches

There is a broad range of ways to attach proteins to immobilization surfaces. The immobilization surface, sample matrix, protein property, buffer ingredients, and assay performance metrics all play a role in determining a particular immobilization technique (e.g., sensitivity, reusability, selectivity, and reproducibility). For a high-performance, repeatable experiment, protein structure must be maintained after immobilization. Methods for immobilizing proteins may be classified according to the molecular mechanism they use, which can be adsorption, bioaffinity interaction, covalent binding, or a mix of these three procedures [95 - 97].

The most straightforward and cost-effective technique for immobilization is physical adsorption, often known as physisorption. It is dependent on a nonspecific kind of physical connection between both the protein and the transmission surface, such as a hydrogen bond, an ionic bond, or the forces of Van der Waals. Changes in temperature, pH, and ionic strength can cause proteins to desorb from their binding sites; however, because the interactions involved are generally weak, it is not uncommon to observe this process taking place. Other drawbacks include the disorderly orientation and the subsequent nonspecific adsorption of other proteins or other compounds, which are more accurately referred to as nonspecific binding. Strong adsorption can be seen for proteins on hydrophobic surfaces. It is common for the protein structure to spontaneously unfold, increasing the hydrophobic part of the polypeptide chain that is in interface with the carrier. In many circumstances, this spontaneous thermodynamic process results in antibody denaturation and loss of activity [95 - 97].

The other way to immobilize antibodies is via the covalent coupling method. This approach provides a more stable attachment of the biomolecules to the substrate surfaces than the previous method. It is extremely stable in a broad variety of circumstances, including chemical (e.g., pH) and physical (e.g., temperature) variables. Specific functional domains in the protein are targeted by this method. Amino acids, which include both amino (-NH2) and carboxyl (-COOH) groups, are well-known as the basic monomer units of protein, and the functional groupings distinguish individual amino acid units. In addition to hydroxyl (-OH) and thiol (-SH) groups, disulfide (-S-S) groups, methyl, isopropyl, and isobutyl groups, and acid groups are also considered functional. The majority of the functional groups that are identified on the surfaces of the substrates are hydroxyl (-OH), silanol (-SiOH), carboxyl (-COOH), and amino ($NH_2$). Before protein can be immobilized on a surface, it is often subjected to some kind of chemical treatment [95 - 97].

For the fabrication of biosensors, a variety of carrier materials are available, and the native surface properties of these materials may require a chemical modification depending on the immobilization method that is chosen and the characteristics of the antibody that is to be bound. Thiols, silanes, and their derivatives are all accessible with a wide variety of functional terminations; nevertheless, it is possible that additional changes to the surface characteristics may be required. These replacements can be done via a wide variety of chemical processes [95 - 97].

There are a number of different groups that may be linked to the carboxyl terminus of the antibody molecules, including phenols and thiols, but the most common is the amino groups existing in their structure. Even if there are a few surfaces tyrosine,

cysteine, or histidine residues present, the bulk of bonds that result from the coupling of antibodies will be with surface amino groups of lysine residues. This is because tyrosine, cysteine, and histidine residues are often far less numerous than lysine residues [95].

As shown in Figure 2.4 [97], There are typically two ways to generate the amide bond. The first method involves activating the carboxylic group with a carbodiimide

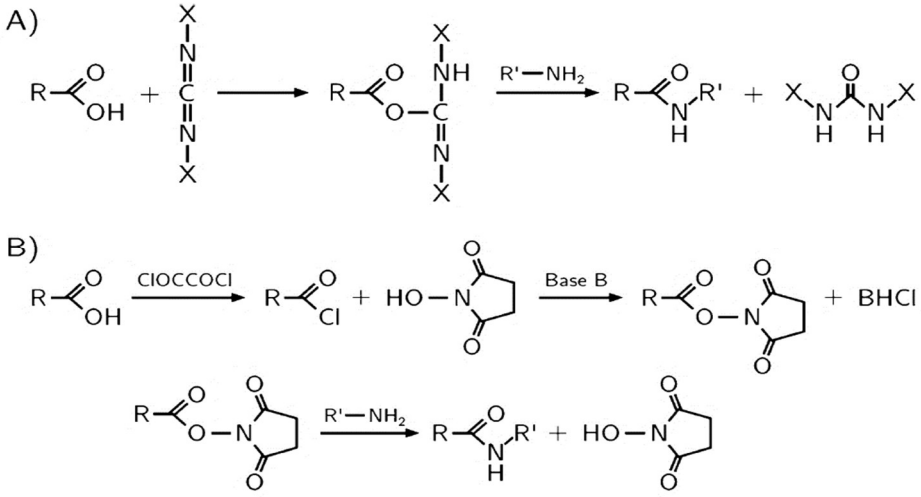


Figure 2. 4 A) Formation of an amide bond. B) Two-step formation of amide bonds via NHS

reagent such as 1-ethyl-3-(-(3-dimethylpropyl)-carbodiimide (EDC), which subsequently attaches to an amine. The second method involves activating the carboxylic group with a carbodiimide reagent such as 1-ethyl-3-(3-dimethylpropyl N-hydroxysuccinimide (NHS) and acid chloride can also be used to turn the carboxylic group into an "active ester," and then the amide can be produced again by reaction with an amine [96,97].

The immobilization of antibodies through covalent coupling results in an irreversible process that allows for a substantial increase in surface coverage. In

comparison to the adsorption process, the covalent coupling method has a number of benefits, the majority of which contribute to the increased sensitivity, improved reproducibility, and increased lifetime that characterizes the method. The process of covalent coupling has a number of potential limitations, one of the most significant of which is the possibility that the procedure will have an effect on important functional groups of the protein, which could lead to the protein losing its bioactivity. Furthermore, a wide variety of reagents have the ability to react with amino groups. The presence of several amino groups in most protein chains makes it difficult to target reagents to individual amino groups. Another disadvantage of the covalent coupling method is that the immobilized protein can be linked to the surface in an excessively tight fashion, which may cause steric interference between the proteins.

### 2.4.4 Self-Assembled Monolayers (SAMs) Methodology

As previously mentioned, the antibody can be immobilized on a surface by the use of straightforward and easy procedures, such as the physical adsorption approach and the covalent coupling method. They can be easily eliminated by the buffer used in the experiment because of the weak, pH-dependent adhesion. There is also the possibility of entrapping biomolecules within electrodeposited molecular layers of polyphenol, polythiophene, or polyaniline [97]. In this particular instance, molecules are expected to diffuse in and out of the layer. The better the sensing, the faster the diffusion will be hence thinner layers, or several layers are preferable.

The spontaneous creation of ordered structures or patterns from elementary units is what is meant by the word "self-assembled," which defines the phenomenon. The natural world contains a considerable amount of it (e.g., lipid membrane, cells,

organisms). Along with its affinity for the "head group" of molecules, a SAM spontaneously develops on a suitable substrate. During the process of SAM formation, direction and structure are achieved through interaction between a hydrophilic "head group" and a hydrophobic "tail group." The tail group offers resistance against chaining while also ensuring the development of a monolayer and preventing the formation of a multilayer structure at the same time. In a subsequent step, the negative group (the Greek letter "omega" is used in chemistry for the end group of a chain, also known as the "tail") can be switched to a different one for a convenient linking to a suitable biorecognition element, as illustrated in Figure 2.5 [97].

The viability of SAMs for use in the creation of competitive biosensors can be considered as a rapid and easy immobilization method for a planar substrate in the laboratory. It can be achieved by soaking the substrate in a diluted solution of an organic molecule for a certain amount of time, then thoroughly washing the substrate with the same solvent and drying the substrate in the presence of a flow of nitrogen. In addition, the creation of a self-assembled monolayer requires just a very relatively small amount (about $2 \times 10^{-7}$ $gcm^{-2}$) of chemicals. Therefore, from an economic perspective, it is

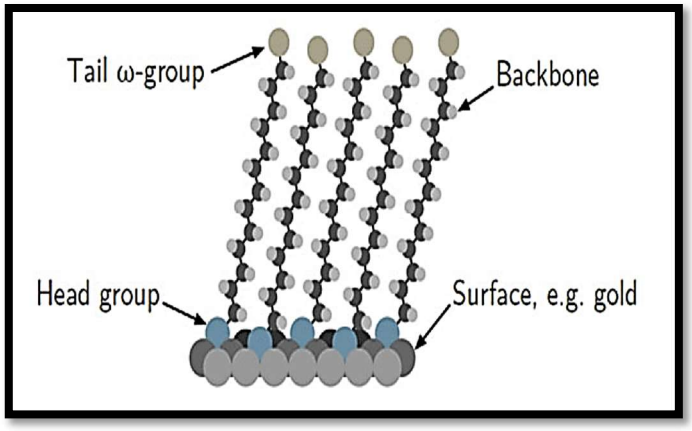


Figure 2. 5 SAM formation on a surface

reasonable to use even pricey chemicals in the process of developing SAM-based biosensors for use in service environments [96, 97].

The functional groups of the molecule and the characteristics of the surfaces both have a role in the formation of self-assembled monolayers, which can take place on a variety of different surfaces. However, the monolayer creation technique should be based on the physicochemical features of the surface and biomolecules. It is important that the active biomolecules maintain their structural integrity once they're on the surface for a significant amount of time. For this reason, siloxane on silicon and thiols on gold surfaces have attracted great attention. Trichlorosilane is a regularly used solvent for forming a monolayer on silicon during the assembly process. It has polar o-functionalities on the linear hydrocarbon, such as OH or $NH_2$, is extremely reactive and incompatible with an aqueous solution. In addition, it is possible to make use of relatively nonreactive substituents such as hydrocarbons (alkane, alkene, or alkyne), as well as halogens. On the other hand, the creation of SAMs on the surface of gold requires the terminal thiol of the

molecule to be able to tolerate functional groups such as OH, COOH, and $NH_2$ within the molecule. In addition, contaminants that were only weakly adsorbed are pushed away from the surface of the gold by the sulfur-containing chain. Order and crystallinity of the SAM are two crucial factors that must be taken into consideration to achieve maximum activity of the biomolecule in the biosensor. It was found that when a monolayer is produced using long chain alkanethiols (the number of methylene groups must be larger than 10), the order and crystallinity of the substance are improved [98].

In order to attach a biomolecule to a SAM, either a covalent bond or a non-covalent association needs to be formed between the biomolecule and the exposed functional terminal of the SAM. Despite the fact that non-covalent attachment typically allows for a more delicate procedure, there is always a high probability that the concentration of the active component on the matrix may progressively decrease with repeated usage and washing. Contrarily, a longer period of time can be tolerated by molecules that have been covalently bonded. The accessibility of a monolayer's end group should be high in order to maximize the covalent and non-covalent attachment of biomolecules to SAMs. To improve the accessibility of the key functional group in the bulk medium, it is standard procedure to insert a spacer unit between the exterior termini of the alkyl chain and the key functional group. Common examples of spacer units include triethylene glycol and hexaethylene glycol [95- 99].

The construction of a biosensor requires careful consideration when selecting an appropriate approach because the activity of biomolecules can be reduced when their natural structures are deformed or randomly oriented. Numerous techniques for attaching biomolecules on SAMs on surfaces have been developed during the past few decades.

Attachment can occur in one of two ways: either through a non-covalent contact (such as electrostatic, hydrophilic, or hydrophobic) between biomolecules and the head groups of the SAM or through the creation of a covalent bond between biomolecules and the head groups of the SAM. Both of these attachment mechanisms are possible. Methods that involve affinity interactions, such as antigen-antibody interactions or biotin-avidin interactions, also fall within the first group. They incorporate various points of interaction, each of which is non-covalent in nature and contributes a significant amount of binding energy to the system [95- 99].

2.5 Binding Methods for spike glycoprotein to the Biosensor

Salinization is an immobilization method that is essentially another type of SAM since this class of chemicals can also result in monolayer formation on designated surfaces. However, silanes differ from their thiol-based counterparts in several aspects. First, they can provide covalent bonds between both the substrate-chemical and chemical-protein interactions. In the field of protein immobilization, the representative formula used to designate a silane is as follows: Salinization is an immobilization technique that is essentially another kind of SAM due to the fact that this family of chemicals may likewise result in the development of monolayers on certain surfaces when used. Silanes, on the other hand, vary from their thiol-based cousins in a number of ways [43]. Second, they have the ability to form covalent connections between both the substrate-chemical contacts and chemical-protein interactions. Silanes are defined by the following typical formula, which is used in the area of protein immobilization to identify a silane: $R^1$-Si-$(CH)_n$-$R^2$, where $R^1$ is typically a methoxy (-$OCH_3$), ethoxy (-$OCH_2CH_3$), or halogen (i.e., Cl) group, Si is the silicon group that serves as the foundation for the chemical's

ability to be a silane, $(CH)_n$ is the carbon chain that can be of any length (three to 10 carbons is commonly used in protein binding research), and $R^2$ is the end group [amine (-$NH_2$). Epoxy SAMs based on silane have traditionally been used to create covalent interactions with metal substrates, such as alkali metals such as Al, platinum, silicon, and titanium, that contain hydroxyl (-OH) and/or oxide (-$O_2$) groups accessible on the outermost surface of the substrate. Because it is a very reactive reaction, some researchers choose to do this experiment under anhydrous circumstances. Considering that the covalent nature of this approach makes it an attractive path to explore, several researchers have attempted to insert the required –OH or –$O_2$ groups into the substrate in the immobilization area by means of substrate modification [43].

A typical method of initiating this process is to include sputtered or plasma deposited elements (for example, silicon dioxide or silicon trioxide), but the pre-chemical alteration is also used sometimes (i.e., substrate-chemical with hydroxyl end groups-silane binding). While $R^1$ is commonly a methoxy (-$OCH_3$), ethoxy (-$OCH_2CH_3$), or halogen (i.e., Cl) group, Si is the silicon group that is the foundation for the chemical being a silane, $(CH)_n$ is the carbon chain that is of variable lengths (three to ten carbons is used extensively in protein binding research), and $R^2$ is the end group (i.e., amine (-$NH_2$), epoxy, thiol (-SH)) that binds covalently with the protein of choice. Traditionally, silane-based SAMs form covalent reactions with metal substrates (i.e., Al, Pt, Si, Ti) that have a hydroxyl (-OH) and/or oxide (-$O_2$) groups available on the outermost surface of the substrate. Since the covalent nature of this method makes it a desirable avenue to pursue, when a substrate in the immobilization region does not have the necessary –OH or –$O_2$ groups, some researchers introduce the essential groups with substrate

modification. This is usually initiated through the incorporation of sputtered or plasma deposited materials (i.e., $SiO_2$, $Si_3N_4$) or even less frequently with pre-chemical modification (i.e., substrate-chemical with hydroxyl end groups-silane binding) [43].

SAMs may be produced on a wide variety of substrates, including glass, silica, ITO, gold, polymers, and metals, which are utilized for the vast majority of practical applications. As shown in Figure 8, the surface wettability (hydrophobicity) of SAMs is controlled by the surface functional groups (X) of the SAMs. Amine and carboxylic SAMs have been shown to be hydrophilic, having water contact angles of 62 2° and 40 2°, respectively, according to the literature. Using hydrophobic, methyl, and octyl (alkyl) SAMs, a contact angle of less than 100° was achieved. The wettability of a mixed and hybrid SAM was 80 2°, which was considered moderate. In the study of SAM production, it was discovered that there are two steps: a fast attachment followed by a gradual rearrangement. In one study, it was discovered that the reaction time might be used to regulate surface coverage, resulting in the formation of surfaces with various wettability. Another method for tuning the surface wettability is to create mixed SAMs that include both hydrophilic (such as COOH and NH2) and hydrophobic (such as CH3) groups [43].

Following analysis of the spike protein's biophysical chemistry, it seems that a mixed SAM composed of COOH and $CH_3$ groups would be the most effective for achieving strong and precise attachment/binding of the spike S1 protein. Combining aminopropyl triethoxysilane (APTES) and triethoxy(octyl) silane TEOS, mixed (amine-octyl) SAM was created by immersing the hydrolyzed

surfaces in a combination of aminopropyl triethoxysilane (APTES) and triethoxy(octyl) silane TEOS. This equation, which determines the surface energy of mixed SAMs, is known as the Cassie equation [43].

Self-assembled monolayers (SAMs) are studied in this approach to create nanostructured surfaces with a broad variety of weathering conditions (hydrophobicity). SAMs are spontaneously generated on a surface by covalent attachment without affecting the material's mass characteristics. A wide variety of substrates, including the use of appropriate surface modifying agents, include SAMs such as glass, silica, indium tin oxide (ITO), gold, Polymers, and metals [43].

Furthermore, current research showed the ability to analyze the new coronavirus (SARS-CoV-2) via various channels, including anal swabs, blood, and oral swab, in addition to traditional methods. This research defined the serology test with an eye on future epidemiology and disease outbreaks. Another study revealed the presence of SARS-CoV2 as well as other respiratory viruses in nasal and throat swabs as well as sputum samples, according to the findings [43]**.** As a result, utilizing engineered surface-based methods, the presence of the coronavirus in an oral swab may be simply and precisely detected and identified. These designed surface chemistries may be applied on a quartz crystal, and detection can be carried out using a quartz crystal microbalance, as previously mentioned (QCM). According to the Sauerbrey equation, the reduction in the crystal's vibration frequency (F) is exactly proportional to the decrease in its mass. QCM has been investigated for the purpose of studying the adsorption behavior of

various proteins on different SAMs in order to determine the quantity of adsorbed protein, the degree of competitive adsorption, and the viscoelastic characteristics of the adsorbed layers [43].

Antibodies (anti-spike glycoproteins such as immunoglobulin (Ig) and camelid heavy-chain antibody (VHH) may be immobilized on the modified surfaces in order to enhance specificity. In order to detect high molecular weight protein hIgG, several SAMs have been used to covalently couple the anti-immunoglobulin G (anti-hIgG) to the hIgG antibody. These rehashes used straightforward the chemistry of 1-Ethyl-3-(3-dimethylaminopropyl) carbodiimide/N-Hydroxysuccinimide (EDC/NHS) to immobilize antibodies on modified surfaces via the creation of amide linkages. In the presence of SAMs, it was discovered that the sensitivity had been increased, and the detection limit had been reduced. An electrochemical immunosensor based on amine self-assembly was developed for the detection of the Zika virus protein [43]. In addition, a mixed SAM was utilized to immobilize antibodies for the particular detection of Escherichia coli successfully. The sensor proved effective in detecting E. coli when used in conjunction with a direct assay and a protein G-based test, with limits of detection reported to be $10^6$ CFU/ml and $10^4$ CFU/ml, respectively, in both assays. In a similar vein, a mixed self-assembled monolayer with lectin protein functionalization was used to detect E. coli [43]. This demonstrated that mixed SAMs, either alone or in combination with an antibody (anti-spike glycoprotein), were effective in attaching to and adsorbing the new coronavirus

through its spike protein. In order to determine the sensitivity and detection limit, it is necessary to conduct experiments.

According to the results, the PI of the spike S1 glycoprotein is less than 6.0. The pH of serological (swab) samples may thus be adjusted below 6 (the PI of the spike protein) in order to enhance electrostatic interactions with negatively charged surfaces, therefore increasing selectivity. Furthermore, surface-modifying compounds derived from polyethylene glycols (PEG) such as PEG silanes and PEG thiols may be investigated in order to reduce biofouling of the designed surface and nonspecific adsorption. Using oligo (ethylene glycol) (OEG) and integrating p-mercaptophenylboronic acid (PMBA) and p-aminothiophenol, glycoprotein imprinted mixed SAMs have recently been developed (PATP). Using hydrogen bond binding, these mixed SAMs demonstrated high recognition selectivity for target glycoproteins.

# CHAPTER THREE

# SURFACE ACOUSTIC WAVE BIOSENSOR DESIGN AND MODELING

## 3.1 Surface Acoustic Wave Sensor (SAW) Physical Design

### 3.1.1 SAW Sensor Basic Parameters

As discussed earlier, all surface acoustic wave sensors need a piezoelectric material to convert electrical impulses into mechanical stress and back again [100]. Due to collisions between negatively and positively charged molecules in the 3D structure of piezoelectric material, a piezoelectric material's positive (+) and negative (-) charges are simultaneously eliminated. The internal structure of the piezoelectric material is exaggerated when pressure is exerted to its surface, producing the negative charges at its upper and lower ends to come closer together. As a result, the structure becomes electrically polarized [100].

Figure 3.1 [100] depicts a characteristic SAW device structure component consisting of interdigitated electrode IDTs on a piezoelectric substrate. In addition, thin metal films with typical thicknesses ranging from 50 to 200 nm are used to pattern the interdigital transducers IDTs fingers on both the devise substrate and the thin film. The standard photolithography process can be used to deposit metals on the substrate. Numerous designs and various layouts of the interdigitated electrodes are achievable based on the target application and the

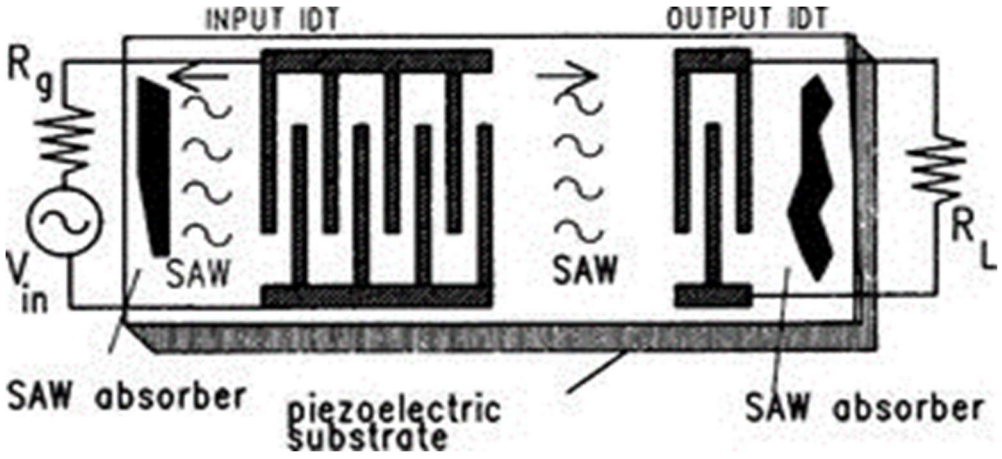


Figure 3. 1 Outline of a primary SAW filter on a piezoelectric substrate

user's particular needs. Moreover, efforts were made to accomplish the critical and distinctive design of IDTs in order to decrease insertion loss and obtain high center frequency responses. Electrode width, spacing, aperture, and the number of fingers significantly influence the designed IDT's frequency bandwidth and electrical impedance[100].

Using a piezoelectric material, a SAW sensor transmits an oscillating electric frequency between two interdigital transducers (IDTs) at different distances. The input IDT operates as a transducer, converting an electrical signal into a surface acoustic wave signal, which the output IDT receives the acoustic wave and transforms it into an electrical signal. In contrast, the transducers are designed for electro-mechanical transduction and should be constructed to convey a specific amount of energy at a given frequency. As a stress wave travels through the material, mechanical energy is transmitted via electro-mechanical

transduction. Thus, the transducers influence the phase, amplitude, and frequency of the stress wave that will be developed in the substrate [1,4,29,28].

In addition, an insertion loss and a frequency shift in the output signal are induced when a thin chemical selective polymer film is introduced between the IDTs on a SAW. If the polymer coating is subjected to organic molecules or chemical vapor that can be absorbed into the polymer materials, the film's mass loading and elastic characteristics will modify, resulting in a further insertion loss and frequency shift. On the micro-scale, the IDT's coupling with the piezoelectric material is the primary emphasis for reducing loss [1,4,29,28].

IDTs are designed in such a way that their primary focus is on developing a central frequency through transduction, the reduction of reflection, regeneration, and access to higher harmonics. These parameters might be altered by adjusting the electrode parameters as follows: electrode width (w), spacing (s), aperture (W), number of fingers (N), and apodization [28, 29].

Research into earlier designs has yielded a great deal of valuable information in developing a new model. The center frequency (f) is lower when the electrode width (w) is higher. To reduce reflection, spacing (s) and width (w) should be equal in length to the wavelength of the wave created. The common IDT spacing for most devices is a multiple of an integer or one half, one third, or one-quarter of the wavelength as:

$$\lambda = \frac{2\pi}{k} \tag{3.1}$$

where k represents the wavenumber traveling parallel to the direction in which the wave travels. Another method for determining the acoustic wavelength is to use the equation that is as follows:

$$\lambda = \frac{c}{f} \tag{3.2}$$

where f is the surface wave's resonance frequency, and c is the phase wave's velocity [1, 8, 29]. The wave amplitude increases as the number of fingers rise because the aperture (W) decreases. When more fingers are added to the SAW sensor, its harmonic output grows within one wavelength. The period L regulates the number of harmonics created by changing the finger width (w) to the period (L) ratio. Capacitance is produced by the interdigitated electrodes, which function as a system. The overall capacitance can be calculated using the IDT configuration as follows:

$$C_{Total} = \frac{1}{2\pi f Z} \tag{3.3}$$

where Z is an indicator of the IDT's impedance [4, 28]. It has been demonstrated that the IDT's impedance should match the impedance of the entire measuring system for the greatest responsive results. In addition, the IDTs' aperture (ap) is critical. Aperture W for the IDT system's overlapping fingers is provided by:

$$W = \frac{C_{Total}}{C_{0*N}} \tag{3.4}$$

where N is the number of IDT fingers in total.

The insertion loss and the central frequency $f_0$ of a SAW device are also extremely critical when it comes to the sensing function of the device. In particular, a SAW-based sensor with a high level of sensitivity has to have a

central frequency in the megahertz and gigahertz region. Nevertheless, insertion losses are incurred by the system as a consequence of this performance. SAW devices have the capability of functioning as passband filters.

Wavefront transmission speed is dictated by the stiffness constant and mass density of the propagation medium, which is fundamentally determined by the acoustic wavelength of SAW and SAW mode phase velocity $v_0$ [101]. It can be seen that their relationship is as follows:

$$f_0 = \frac{v_0}{\lambda} \tag{3. 4}$$

According to equation (3.4), the SAW sensor is more sensitive when the operating frequency of the SAW sensor is larger, which is primarily related to lower wavelength and more energy of SAW can be trapped to the surface. For a SAW, the type of acoustic waves depends on the piezoelectric sensor material, cut type, and frequency of IDT fingers. The sequence of these three aspects determines the characteristics of the waves generated by a SAW [102].

Since the SAW propagation is not isotropic but rather anisotropic, researchers shall seek a dominant wave capable of encoding information most effectively as it moves from the input IDT to the output IDT. There is the potential for both electrical potential and mechanical deformation to be generated by a surface acoustic wave (SAW) while it is propagating through a piezoelectric medium. As a result, the opportunities for both electrical and mechanical couplings between the SAW and the surface layer.

The major responses of SAW to internal perturbations, including temperature, elasticity, and stiffness, or external perturbations, including stress, mass loading, viscosity, or conductivity change. In this way, they may be summarized into acoustic

wave velocity (v0) and attenuation (Δα), which are inherent features of SAW. SAW's sensitivity to various perturbations can be estimated by taking measurements of v0 and Δα.

Upon perturbations, mass loading, elastic and viscoelastic effects of SAW devices are mechanical coupling effects. Within these effects, the mass loading effect is most widely used for SAW sensor applications based on the mess density (mass/sensing area) change on the surface of a SAW device [103]. A thin and rigid layer on the surface moves synchronously with the SAW, causing an increase in the kinetic energy density, and this is expected to change the wave phase velocity without bringing the attenuation on SAW mode. With too thick or elastic film loading, the velocity and the attenuation of SAW mode will be changed.

As specifically mentioned, one of the most significant factors that makes SAW devices unique is their extraordinarily high sensitivity. However, when sensing in liquid environments, SAW devices feature the surface normal displacement component, which leads to substantial energy radiation to liquid [104]. According to a recent study, the typical SAW suffers from substantial signal attenuation in liquid environments because of the interaction between its shear vertical component and the liquid [104]. Because of that, the limitation of the SAW mode can be addressed by utilizing alternative shear-horizontal (SH) acoustic wave devices. As a result, it is necessary to use acoustic waves with particle displacements normal to the wave propagation direction and parallel to the surface of the device [28,29].

The design of SH-SAW devices is the same as that of SAW devices; the only differences are in the materials used, the crystal cuts, and the directions in which the

waves propagate. As a rule of thumb, SH-SAW can be developed while adjusting the ideal SAW's boundary conditions in the majority of circumstances. SH-SAW can generate while adjusting the ideal SAW's boundary conditions in most cases [105,106]. The SH-SAW mode is intrinsically linked to both longitudinal and shear-horizontal components. Like SAW mode, this mode's energy tends to be concentrated near the ground. As a result, it is highly agitated, travels close to the surface, and is easily influenced by surface perturbations.

In most cases, the phase velocity of SH-SAW mode will be greater than that of SAW [101]. The SH-SAW mode can be used for aqueous sensing without sacrificing the SAW mode's high sensitivity. In point of fact, the SH-SAW sensor can be applied not only in gaseous settings like SAW but also in aqueous environments for purposes such as environment monitoring, manufacturing process management, and biosensor technology [103]. Other types of acoustic wave devices, such as TSM and APM, also exhibit SH polarization and have been utilized effectively in the field of liquid sensing. On the other hand, due to the nature of TSM and APM, which both involve bulk acoustic waves [107], [108] achieving a high sensitivity level with either method is incredibly challenging. Consequently, SH-SAW devices are considered the most promising preferences for acoustic wave sensing in aqueous environments [109–111].

### 3.2.2 Thin Film/Substrate Materials Structures

Several anisotropic materials, particularly those without a central symmetry, exhibit piezoelectricity. Quartz ($SiO_2$), lithium tantalite ($LiTaO_3$), lithium niobate ($LiNbO_3$), sapphire ($Al_2O_3$), lead zirconate titanate (Pb (Zr, Ti)$O_3$, PZT), aluminum

nitride (AlN), zinc oxide (ZnO), gallium nitride (GaN), silicon carbide (SiC), and indium nitride (InN) are some of the raw materials that fall under this category [112].

PZT has the highest electro-mechanical coupling coefficient, whereas AlN has the highest wave velocity among these materials. Quartz is utilized extensively as a result of the unusually low-temperature coefficient of frequency that it possesses. Consequently, quartz possesses excellent thermal stability, making it suitable for sensitivity sensing applications. It is possible to construct Rayleigh SAWs on substrates made of 128 Y-X-cut $LiNbO_3$ and X-112 Y-cut $LiTaO_3$. SH-SAW can be developed on 36 Y-X-cut $LiTaO_3$ substrates, 64 Y-X-cut $LiNbO_3$, and $Al_2O_3$ substrates. As a result, these devices are typically utilized for sensing in liquid media or high humidity conditions since the polarization of the acoustic wave is nearly horizontal, reducing acoustic radiation into the liquid [112].

These substrate materials and the widely utilized ST-cut quartz are popular choices when fabricating several Love-mode SAW devices. The majority of acoustic devices are built from bulk piezoelectric materials; however, these materials are typically expensive and cannot be easily combined with electronics for control and signal processing. Additionally, they are often brittle and weak when polished into extremely thin structures for high-frequency applications [112].

Acoustic wave technologies based on piezoelectric thin-film materials such as ZnO, AlN, and PZT are regarded as one of the most important technologies for future acoustic fluidics and Lab-on-a-chip devices. Indeed, these applications utilize thin films instead of expensive and fragile bulk materials or substrates; microelectronics, sensors, and microfluidics can be easily and affordably integrated into a single LOC device. The

piezoelectric thin film also permits the integration of several functions onto different substrates, such as silicon, glass, metal, or polymer. These piezoelectric films can be used to make a variety of flexible and wearable sensors, as well as tactile transducers and energy harvesting devices based on polymers [112].

Another important advantage of piezoelectric thin films is that the film can be deposited just on the parts that require the acoustic wave. This makes it possible to limit the film's coverage to just the necessary locations. Once the wave has been formed, it is able to propagate along the substrate even without the need for the piezoelectric top layer. This means that the piezoelectric film does not need to be deposited onto additional locations. So, other components, such as microchannels, chambers, and sensors, can be directly produced on the substrate in this manner without the need for piezoelectric films. A major simplification of SAW devices and microsystems is achieved through the selective deposition of the piezoelectric film, which also avoids direct contact between the active layer and the liquid [112].

ZnO and AlN are the two thin-film materials most widely used in SAW-based microfluidics and LOC devices. Other materials are being studied for piezoelectric applications, including gallium arsenide (GaAs) as well as polyvinylidene fluoride (PVDF); however, their electro-mechanical coupling coefficients are low. Due to its high acoustic velocity, high frequency (GHz range), and compatibility with microelectronics and CMOS, GaN films have often been used to fabricate SAW and Lamb wave devices as well as other high-frequency devices. Thin films of $LiNbO_3$, $LiTaO_3$, $KNbO_3$, $SrTiO_3$, $BiFeO_3$, and $BaTiO_3$ have also been examined for Lamb waves, SAW, BAW, or FBAR devices because of their electro-mechanical solid coupling coefficients; however, these

films frequently suffer from poor control of film lattice constant, orientation, texture, and process parameters [112].

AlN is a material that is stable at high temperatures and possesses excellent mechanical characteristics. Furthermore, AlN can keep its piezoelectric capabilities even at high temperatures, such as 1000º Celsius or 700º degrees Celsius. In addition, AlN possesses a high breakdown voltage, excellent dielectric characteristics, high thermal conductivity, and a sizeable propagating wave velocity. Since higher frequencies and more considerable powers are possible with AlN, novel acoustic devices can be developed with improved sensitivity and performance even at high temperatures and severe conditions. For high-frequency SAW and FBAR devices, AlN films are more appropriate than ZnO. In contrast to ZnO, AlN's deposition and processing are utterly compatible with CMOS and MEMS technologies [112].

When it comes to SH-SAW sensing, a general rule of thumb to follow for the majority of acoustic devices is that the detection sensitivity scales as the square of the operating frequency $f^{2.}$ At higher frequencies, acoustic energy is concentrated more closely to the surface, and the wave's sensitivity to surface perturbations rises as a result. Since the operating frequency is proportional to the acoustic wave's phase velocity, this indicates that to achieve a higher level of sensitivity, it is critical to use a type of material with a higher phase velocity when using the SH-SAW mode.

As was previously noted, various types of piezoelectric materials, such as $LiTaO_3$ [110, 111] and $LiNbO_3$ [113], [114], are able to be utilized for SH-SAW applications. Bulk materials with phase velocities less than 4000 m/s are both suitable for SH-SAW use. When compared to these traditional piezoelectric materials ($LiTaO_3$ and $LiNbO_3$),

Aluminum Nitride (AlN) is a promising material due to its fast acoustic phase velocity and significantly higher electro-mechanical coupling coefficient K [115]. This value is derived from the material's piezoelectricity coefficient, elastic constant, and relative permittivity. Other conventional piezoelectric materials include $LiTaO_3$ and $LiNbO_3$. A high coupling coefficient demands a lower number of IDT fingers to produce a suitable insertion loss, and it also makes it easier to construct devices with more compact dimensions.

3.2.2.1 Characterization of Aluminum Nitride Films AlN

As was stated previously, mathematics demonstrate that the frequency response will be higher when the phase velocity is higher and the wavelength is shorter. On the other hand, the use of materials that have a larger phase velocity is preferred. In addition, AlN possesses several properties, including a linear temperature coefficient [105], strong chemical and mechanical stability, high electrical receptivity [116], high resistance to breakdown voltage, and good thermal conductivity. Because of its structure as a thin film, it is possible to integrate acoustic technology using conventional integrated circuit technology [117]. Furthermore, the thin film structure allows for greater integration with substrate materials to control the phase velocity v, electro-mechanical coupling coefficient $K^2$, and other parameters.

The formation of an AlN layer can be accomplished through the use of RF diode sputtering, metallorganic chemical vapor deposition (MOCVD)[116, 118], and RF magnetron sputtering [119], and plasma source molecular beam epitaxy (PSMBE) [105,120].PSMBE is the process that is most widely used for the deposition of AlN because it can produce high-quality single crystals of AlN at very low temperatures[105].

It has been demonstrated that AlN may be deposited on a variety of substrates, including silicon[121], quartz [122], $LiNbO_3$[123], diamond [124], and $Al_2O_3$ [105]. Compared to the others, $Al_2O_3$ has a lower lattice misfit with AlN than most of them, and its production cost is lower than that of SiC. AlN is frequently employed in the role of substrate in semiconductor-on-insulator (SOI) technology, which adds to the material's appeal for usage in integrating electronic systems based on the Si semiconductor.

SH-SAW may produce synchronously with SAW on thin-film AlN (0001) over substrate $Al_2O_3$ $(11\bar{2}0)$, which is a plane Sapphire, according to research studies that were conducted, and there are numerous distinct propagation directions that can be used. It has been shown that the angular relationship between a thin film and anisotropic substrate planes can cause an extra interaction for the SAW, resulting in the stimulation of new modes in the device when the film thickness is comparable to the SAW wavelength [105]. Based on such a principle, the SH-SAW mode can be generated on an AlN/a-plane sapphire substrate. Both SAW and SH-SAW are excited at the same time on the identical AlN/a-plane Sapphire thin film structure. After both modes have passed through the liquid loading, the SAW mode experiences a significant attenuation. In contrast, SH-SAW is still present despite having a significant attenuation.

The epitaxial relationships are found to be AlN[1100]/Al2O3[0001] and AlN $[11\bar{2}0]$/Al2O3 [1100] according to the experiments of reflection high energy electron diffractions (RHEED). It was observed that the material had a strong resonance of a mode with a higher velocity than typical materials. An investigation into mass sensitivity was carried out using a testing circuit and aluminum (Al) deposition in a magnetron sputtering system. The network analyzer was used to measure the sensor's response in its

natural environment. The mass sensitivity of the AlN SAW mode was calculated to be -173 cm2/g, whereas the SH-SAW mode's mass sensitivity was estimated to be -120 cm2/g. Both modes exhibit a reasonably modest dispersion in conjunction with the thickness of the AlN that was deposited. The rough attenuation of SH-SAW mode with water loading has been studied, and the results showed less attenuation of SH-SAW mode compared to SAW mode. The SH-SAW mode exhibits stronger coupling in certain specific directions than in others. Figure 3.2 (a) [125] illustrates the hexagonal structure and plane orientation of Sapphire, as well as the propagation direction of the SH-SAW mode on AlN/a-plane Sapphire [126,105].

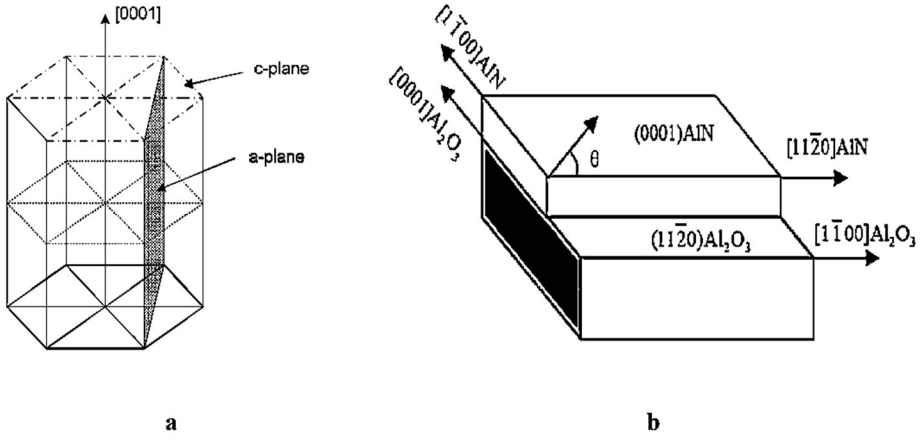


Figure 3. 2 Generation of SH-SAW mode: (a) hexagonal structure and plane orientation of Sapphire, (b) Propagation direction of SH-SAW mode

Finally, in the Smart Sensors & Integrated Microsystem (SSIM) laboratory at Wayne State University, prototypes of SAW and SH-SAW devices on AlN/a-plane Sapphire have been successfully developed [127,128]. There are several benefits to using SH-SAW on an AlN/a-plane, including low attenuation in liquid environments, which makes it a perfect choice for application in liquid sensing systems and biological detection. Therefore, the SH-SAW mode has the capability to be used in the implementation of a biosensing system that can detect bacteria in an environment, including water [125].

## 3.4 Modeling and Simulation SAW device with Multiphysics Software COMSOL

### 3.4.1 Theory Background

In recent times, a growing number of research groups have expressed an interest in the finite element analysis of surface acoustic wave (SAW) devices with a variety of different architectures and designs. All of the simulation models were constructed based on a high-velocity share horizontal surface acoustic wave SH-SAW device that was built on an AlN (0001)/$Al_2O_3(11\bar{2}0)$ structure and had a concomitant high mass sensitivity. The sensing features of the SH-SAW device are explored in this work. The available finite element analysis tool was used to monitor the transmission spectrum of the SH-SAW (COMSOL Multiphysics 5.6). Building an integrated SAW sensor geometry and researching the characteristics of shear horizontal surface acoustic waves are the two things that will be accomplished through reading this article (SH-SAWs).

COMSOL is used to construct a model to prove the concept of employing the spike antibody SARS-CoV-2 as a bioreceptor, which is then immobilized on the SAW biosensor thin film in order to detect the coronavirus (COVID-19) in real-time. Simulated

SAW device frequency analysis was performed using 2D and 3D model simulations with appropriate boundary conditions and input electrical signals, then compared to an actual SAW device that was fabricated and optimized in the clean room.

### 3.4.2 The Use of Mathematical Techniques and Model Structures

After applying voltage, stress-strain relationship equations in nonpiezoelectric materials were used to derive the relationship between piezoelectric stress, strain, electric field, and electric displacement field. This was done after the piezoelectric material was subjected to the electric field. Mechanical stress-strain relationships for tiny static deformations of a nonpiezoelectric elastic material are investigated. Essentially expressed, stress is the force that is exerted on a solid object in proportion to its whole area. In addition to this, stress, force, and area can each be represented as vector values, as the following:

$$T = \frac{F}{A} \tag{3.5}$$

$$S = \frac{\Delta}{L} \tag{3.6}$$

When the force is represented in newtons, the units of T are newtons per square meter ($N/m^2$) (N). In addition, the strain parameter S, which reflects the fractional deformation due to force F, and the fractional deformation of the solid along the length L, are both considered. Compressional and shear stresses and strains can exist within an elastic solid. For example, when compressional stresses are present, the direction of the applied force, denoted by F, is normal to the orientation of the surface area, denoted by A. In any scenario, a proportionate relationship between them is possible according to Hooke's Law for elastic deformations. Hooke's law establishes a linear relationship

between stress, denoted by T, and strain, denoted by S, for stresses and strains associated with simple compression along the same axis, as shown in Equation 3.7.

$$T = c * S \tag{3.7}$$

where c stands for the elastic stiffness coefficient, often known as Young's modulus ($N/m^2$). The strain that occurs in a material as a result of its piezoelectric properties can be represented by the following equations [100,129]:

$$T = -e * E \tag{3.8}$$

Combining equations 3.3 and 3.4 [100,129]:

$$T = (c^E * S) - (e * E) \tag{3.9}$$

where $c^E$ is the stiffness at the constant electric field [100,129].

In addition, the definition of the electric displacement, D ($C.m^2$), for a dielectric material that is not piezoelectric is as follows [100,129]:

$$D = \varepsilon * E \tag{3.10}$$

where ε represents the permittivity ($F.m^{-1}$ = $C.V\ 1.m^{-1}$) and E represents the electric field ($V.m^{-1}$) in the system. The electrical polarization, P that is generated by strain, S, which is defined as a change in dimensions as a result of applied stress, can be described as a model of piezoelectric material that is only one dimension:

$$P = e * S \tag{3.11}$$

where e is the piezoelectric stress constant ($C.m^{-2}$).

$$D = (\varepsilon^S * E) + (e * S) \tag{3.12}$$

where $\varepsilon^S$ is the permittivity at constant strain and S denotes the permittivity while the tension is held constant.

In COMSOL, the piezoelectric constitutive equations were used to describe surface charge density and the relationship between mechanical stress and surface charge, and the results are shown below in the stress-charge form:

$$T_{\mathrm{ij}} = c_{\mathrm{ijkl}} S_{\mathrm{kl}} - e_{\mathrm{kij}} E_{\mathrm{k}} \quad (3.13)$$

$$D_{\mathrm{i}} = e_{\mathrm{ijk}} \mathrm{eijk} S_{\mathrm{jk}} + \varepsilon_{\mathrm{ij}} E_{\mathrm{j}} \quad (3.14)$$

which links the mechanical effect as defined by Newton's law with the electrical impact as dictated by Gauss's law. Where $T_{ij}$ represents the stress matrix, $S_{jk}$ represents the strain matrix, $D_i$ represents the electric displacement vector, $E_k$ represents the applied electric field, and the subscripts I, j, k, and l correspond to the coordinates x, y, and z, respectively. The matrix of elasticity (mechanical stiffness), denoted by $c_{ijkl,}$ the matrix of piezoelectric coupling, denoted by $e_{ijk}$, and the matrix of permittivity, denoted by $\varepsilon$ij, are the material constants that are used as input. Both of the simulation models have 50 pairs of interdigital transducers (IDTs), which are used for the receiving and transmitting ports. The practical devices and the simulation model share the same wavelength (λ), 24 micrometers (μ).

### 3.4.3 The Geometrical Dimensions and Other Relevant Selections

The wavelength λ in this work is selected as 24 μm so that the SAW device operating frequency is around 237.5 MHz- 245.5 MHz, and the SH-SAW device operating frequency is around 251.5 MHz- 258.5 MHz. The thickness of the substrate is 330 um, determined by what wafer is in use, and the thin film thickness is 2 um. The substrate is generally cut as a parallelogram which contains the rectangular area of IDT and electrode parts with a width of 3200 um and a length of 11637 um. In order to reduce

the edge reflection, the substrate shape is cut as not a rectangle. Table 2. Shows the device geometry parameters used in both device fabrication and modeling for this study.

Table 1 Devices Geometry Parameters

| PARAMETERS | (2D) Simulation COMSOL | (3D) Simulation COMSOL | Fabrication |
|---|---|---|---|
| Wavelength (λ) | 24 μm | 24 μm | 24 μm |
| Number of fingers Input/output | 100/100 | 8/8 | 100/100 |
| $Al_2O_3$ Substrate *Width*length*Height* | 333 μm * 150 μm 30 μm | 333 μm * 150 μm * 30 μm | 11600 μm * 3400 μm *330 μm |
| Finger width | 6 μm | 6 μm | 6 μm |

### 3.4.4 2D and 3D Simulation for AlN-based SAW Device

Reconstructing the device's two- and three-dimensional structure in COMSOL using the same design parameters of the realistic model is the most accurate method for simulating the device's performance. However, the existing computer hardware can not deliver sufficient processing power. As a result, in this work, we will simulate a comprehensive 2D model and a simplified 3D model simulation of planar strain.

3D elastic objects can be treated as 2D plane objects with particular limitations and assumptions using plane strain or plane stress analysis. The term "plane stress" refers to a situation where the normal and shear loads are zero in one direction. A plane with

one dimension much less than the other two is assumed to be a three-dimensional object. The two-dimensional planar strain analysis will be implemented as follows. All simulations will be run on a machine with an Intel® Core I7 CPU and 12 GB of memory.

Aluminum Al, Aluminum nitride AlN, and sapphire are the three materials of the device that are considered to be the primary components for the basic structure of our device. All associated materials, including the elastic materials $Al_2O_3$, the piezoelectric material AlN, and the conduct metal aluminum for the IDTs, have been added to the material. The three material models are the piezoelectric material model, linear elastic material model 1and linear elastic material model 2. In the model of the piezoelectric material, we chose the domain representing the AlN layer.

Following a comprehensive series of experiments, the following constants were selected for use in this work. For linear elastic material model 1, all IDT fingers were selected as the domain. The material properties are defined through material tabs where the density is 2700 $kg/m^3$, young's modulus E is 70 GPa, Poisson's ratio is 0.33, and the relative permittivity is 2.2. In the piezoelectric material model, the AlN with the density value of 3260 $kg/m^3$, the young's modulus E is 331 GPa, and the Poisson's ratio is 0.27 was selected as a thin film of the COMSOL model. Figures 3.3 shows the elasticity matrix, Figure 3.4 shows the coupling matrix, and figure 3.5 shows the relative permittivity matrix for AlN that was assigned for both models [127].

Elasticity matrix, Voigt notation

Full

| | | | | | |
|---|---|---|---|---|---|
| 4.1e+011[Pa] | 1.40e+011[Pa] | 1e+011[Pa] | 0[Pa] | 0[Pa] | 0[Pa] |
| 0[Pa] | 4.1e+011[Pa] | 1e+011[Pa] | 0[Pa] | 0[Pa] | 0[Pa] |
| 0[Pa] | 0[Pa] | 3.80e+011[Pa] | 0[Pa] | 0[Pa] | 0[Pa] |
| 0[Pa] | 0[Pa] | 0[Pa] | 1.25e+011[Pa] | 0[Pa] | 0[Pa] |
| 0[Pa] | 0[Pa] | 0[Pa] | 0[Pa] | 1.25e+011[Pa] | 0[Pa] |
| 0[Pa] | 0[Pa] | 0[Pa] | 0[Pa] | 0[Pa] | 1.35e+011[Pa] |

Figure 3. 3 AlN Elasticity Matrix

Coupling matrix, Voigt notation

| | | | | | |
|---|---|---|---|---|---|
| 0[C/m^2] | 0[C/m^2] | 0[C/m^2] | 0[C/m^2] | -0.48[C/m^2] | 0[C/m^2] |
| 0[C/m^2] | 0[C/m^2] | 0[C/m^2] | -0.48[C/m^2] | 0[C/m^2] | 0[C/m^2] |
| -0.58[C/m^2] | -0.58[C/m^2] | 1.55[C/m^2] | 0[C/m^2] | 0[C/m^2] | 0[C/m^2] |

Figure 3. 4 AlN Coupling Matrix

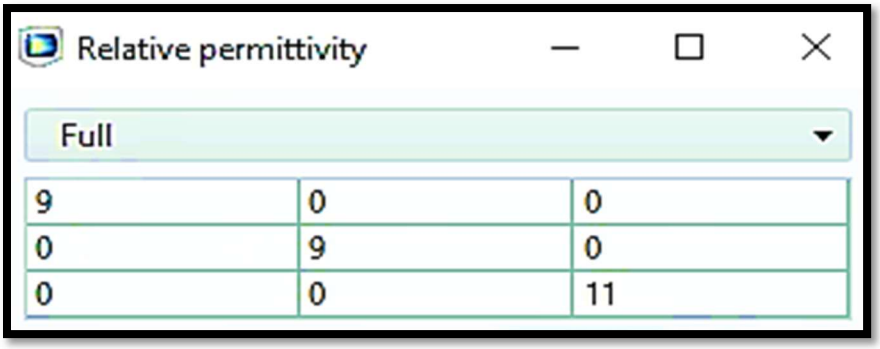


Figure 3. 5 AlN Relative permittivity Matrix

In the linear elastic material model 2, the sapphire substrate with the density value of 3980 kg/m$^3$, young's modulus E is 400 GPa, and the Poisson's ratio is 0.22 was selected as the domain. The anisotropic model is selected as per the sapphire property. Figures 3.6 shows the elasticity matrix, and Figure 3.7 shows the relative permittivity matrix for $Al_2O_3$ that was assigned for both 2D and 3D models [127].

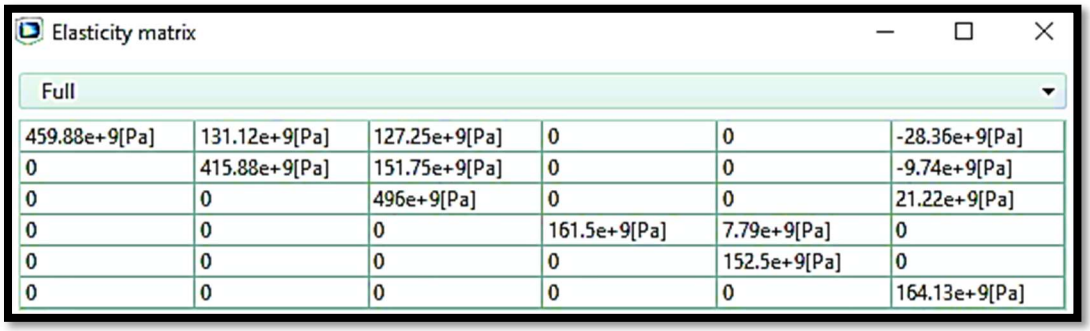


Figure 3. 6 $Al_2O_3$ Elasticity Matrix

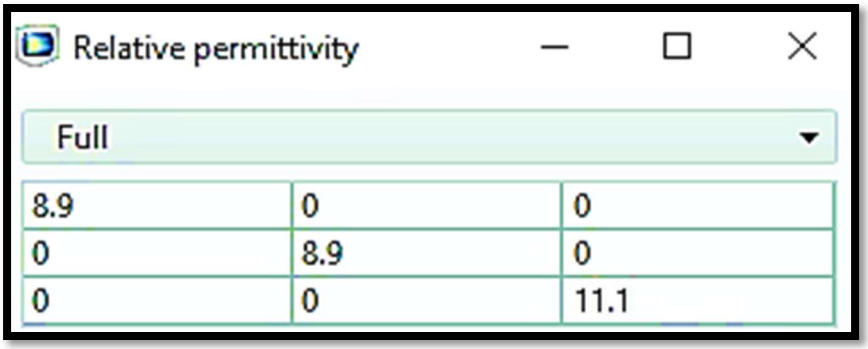


Figure 3. 7 $Al_2O_3$ Relative Permittivity Matrix

The electrical boundary conditions for this study include the zero-charge constraint, the electrical inputs of electrical potentials 1 and 2, and the electrical outputs of floating potentials 1 and 2. The value assigned to electrical potential 1 is 1 Volt, while the value assigned to electrical potential 2 is -1 Volt. For the variables' initial values, the value zero was assigned to all of them. The frequency response is analyzed using the frequency-domain model in the research tab. The frequency range of interest extends from 235 MHz to 260 MHz with a step size of 0.2 MHz. Figure 3.9 (A) shows the essential components for the 2D model with exact dimensions for the geometry structure, and the meshing used in the 2D simulation is shown in Figure 3.9 (B).

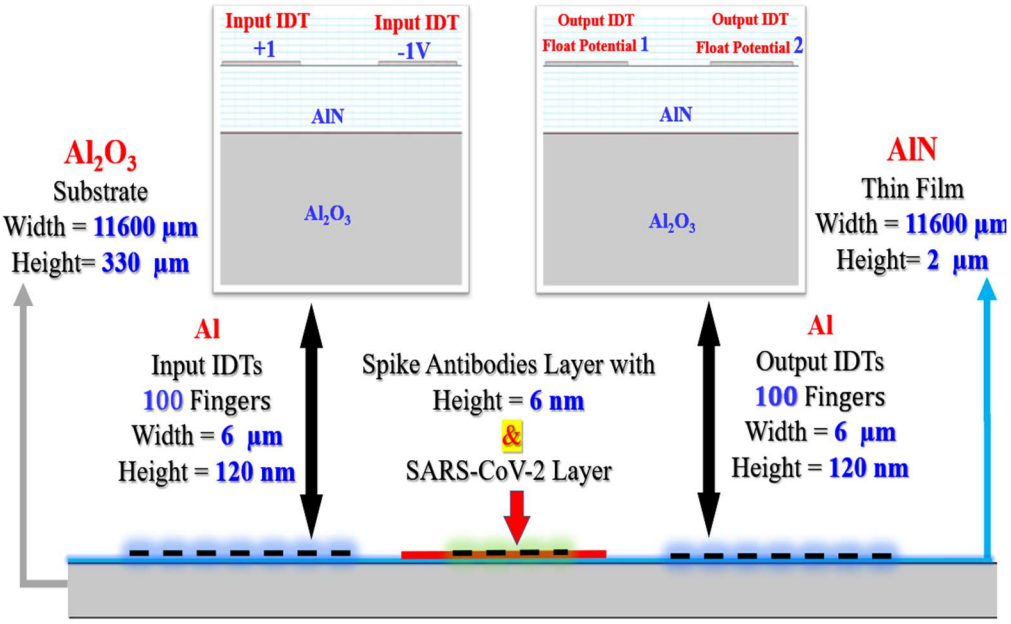


(A)

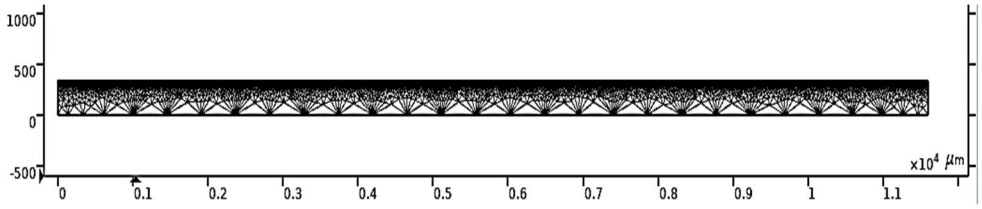


(B)

Figure 3. 8 A) 2D Model for AlN-based SAW Device (Basic Structure), (B) Schematic representation of the meshing used in the 2D simulation

Figure 3.9 depicts the basic components of 3D geometry with an insulating layer for IDT and an APTMS layer between the two IDTs. In addition, the model has meshed before it can be used in COMSOL, and the meshing used in the 3D simulation is shown in Figure 3.10.

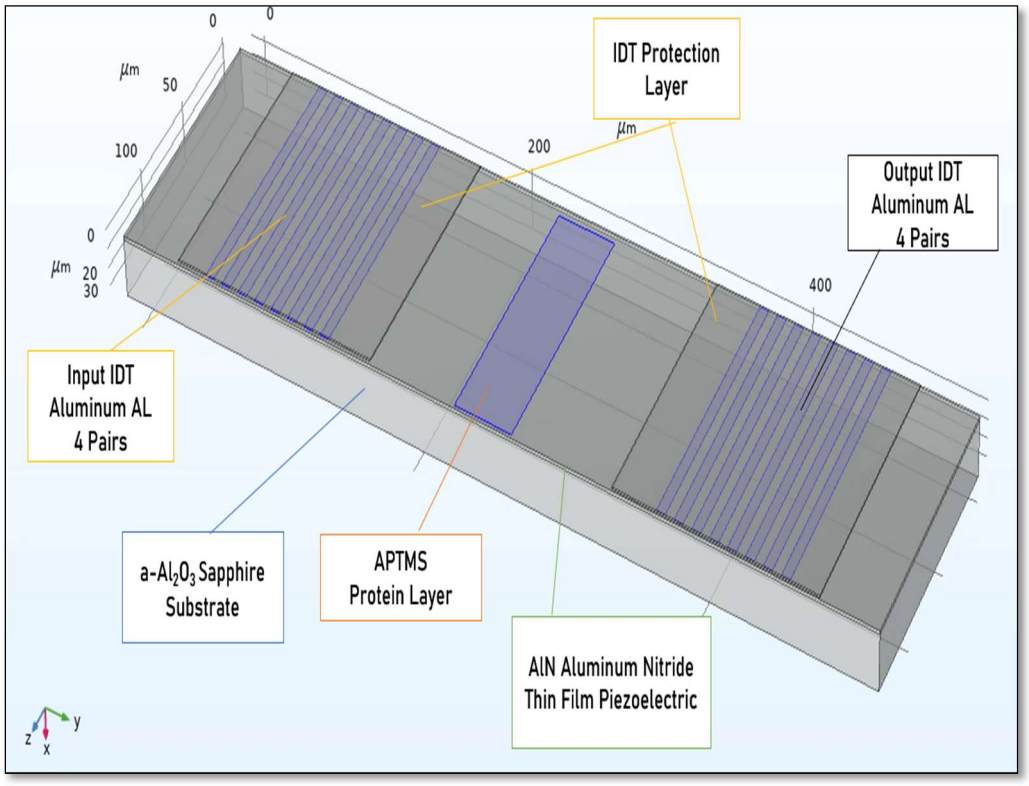


Figure 3. 9 3D Model for AlN-based SAW Device (Basic Structure)

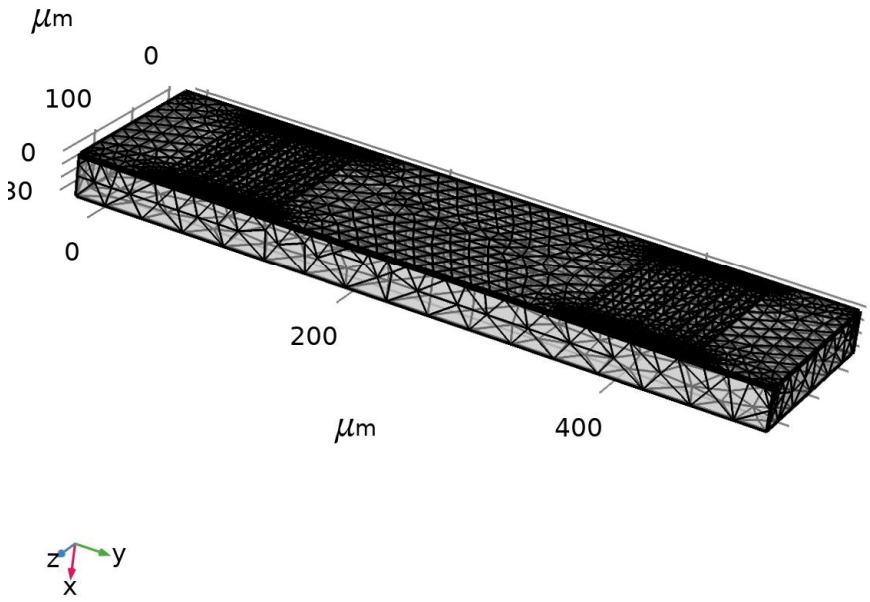


Figure 3. 10 Schematic representation of the meshing used in the 3D simulation

The theory of the physics that determines surface acoustic (elastic) waves is significantly simplified when the material being considered is infinite, homogeneous, elastic, isotropic, and solid. This is accurate not only for the waves themselves but also regarding the theory that describes them. When it comes to the biological layer, none of these features are likely to be present. For instance, in order to establish a soft layer, we can make the assumption that the Lamé constants are lower than 1.0 GPa, that the density is 1000 kg/m3, and that the relative permittivity is 1. When simulating a system, employing the finite element approach has a number of

advantages. One of these advantages is that it is simple to study a range of these parameters in order to find a combination of those qualities that has the greatest perturbative effect [102].

For the purposes of the simulation experiment, the SARS-CoV-2 virus is modeled as an array of blocks, each of which has the ability to bind to the protein layer that APTMS uses to coat the surface sensing region. In order to mimic the total number or concentration of SARS-CoV-2 and the spike antibodies binding to the perception layer, this could be modified by changing the number of blocks in the array. This could be done. A frequency response plot vs. insertion loss dB real indicates any change in the frequency that happens when the protein layer and SARS-CoV-2 are added to the sensing surface area. The working hypothesis is that an increase in the amount of virus that attaches to the protein layer will produce a significant shifting in the resonance frequency as well as the insertion loss for both modes. This shifting may result in an increase in the insertion loss for both modes and a decrease in the insertion loss for both modes too.

Following the installation of a protein-based spike antibody on the surface of the sensing layer (which was connected via a thin attachment layer APTMS), a SARS-CoV-2 virus was created and constructed directly on top of the protein layer. This is interpreted as being representative of the binding relationship that takes place between the analyte and the bioreceptor. This serves as a duplicate of a standard biosensing technology, in which a SARS-CoV-2 spike antibody reacts with the sensor to exhibit an immune response to a pathogen. In this technique, an immune response is displayed in response to the pathogen. Using this method, even minute shifts in the quantity of the spike antibodies linked to SARS-CoV-2 on the sensing area surface ought to result in a

discernible shift in the resonance frequency as well as the insertion loss for both modes of SAW and SH-SAW. This should be the case for both modes of SAW and SH-SAW.

In order to cause mass loading, we use the added mass capability of COMSOL to apply the surface mass density of SARS-CoV-2 in a manner that ensures it is uniformly present over the top surface of the biosensor. This allows us to achieve our goal of inducing mass loading. As was mentioned earlier, the diameter of the SARS-CoV-2 virus ranges between 80 and 90 nanometers. It is possible to model it either as an elastic cylinder rod with a radius of 40 to 45 nm or as an elastic cubic with all of its dimensions being either 90 nm or 80 nm. Both of these models are assumptions. Both the 2D and the 3D models have the same amount of details, and a comparison of the two sets of findings has been taken into account. In the several models that were simulated for this work, SARS-CoV-2 was thought of as an elastic cubic with diameters ranging from 80 nm to 90 nm, a material density of 10.1 $kg/m^3$, and an even distribution across the sensor surface. This was done in order to better understand this virus. During the simulation of the various models, these properties were taken into consideration.

### 3.4.5 COMSOL Simulation Results and Discussion

The main purpose for using the COMSOL is to simulate the sensor for analyzing the effect of the binding interaction between the immobilized bioreceptors and the analyte and the influence of their interaction on the resonance frequency of the sensor. However, the study was based on the previous successful SH-SAW, which was fabricated by our SSIM team in the clean room at Wayne State University. Thus, the reported operating frequency of 243.325 MHz for the SAW mode, while the SH-SAW mode had a reported operating frequency of 256.05 MHz [128].

COMSOL was first used to simulate different scenarios for the SH-SAW biosensor. The first scenario simulated the basic structure of the device that is including the sensor substrate, the deposited piezoelectric thin film, and the input and output IDTs. The second scenario simulated the addition of the antibody coating layer above the sensing layer and between the two IDTs. Finally, the third scenario explored different arrays of the SARS-Cov-2 that are binding to the APTMS coating layer.

Figure 3.11 depicts the insertion loss of the frequency response for both the SAW mode and the SH-SAW mode in 2D simulation as the first scenario. In addition, Figure 3.12 depicts the insertion loss of the frequency response for both the SAW mode and the SH-SAW mode in 3D simulation as the first scenario. When the model was defined with a protein layer that has to be accumulated on the sensing area of the SAW sensor between the two IDTs, the resonance frequency of the basic structure due to the mass loading that loaded in the sensing area was shifted as shown in Figure 3.13. Finally, When the model was defined with a viral layer with different concentrations that have to be accumulated on the protein layer, the resonance frequency due to the mass loading was shifted, as shown in Figures 3.14,3.15 and 3.16.

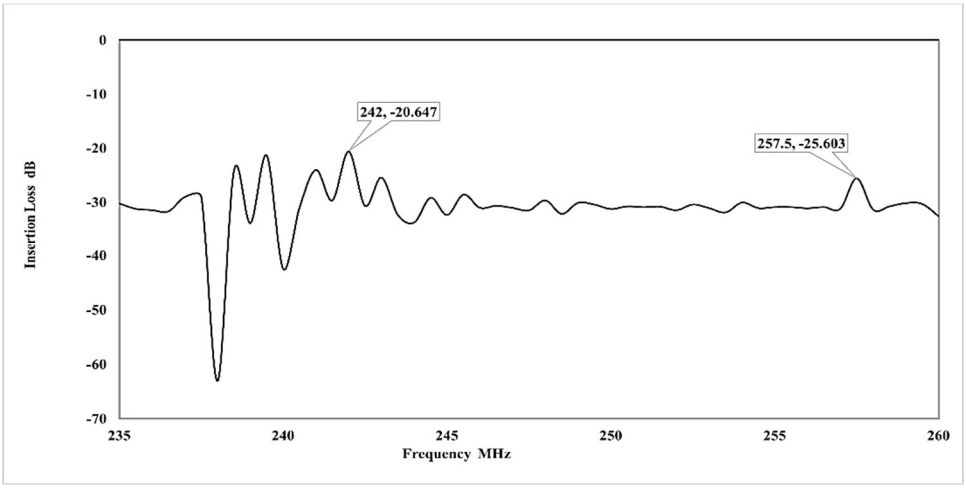


Figure 3. 11 Frequency Response [ 2D Model - Basic Structure]

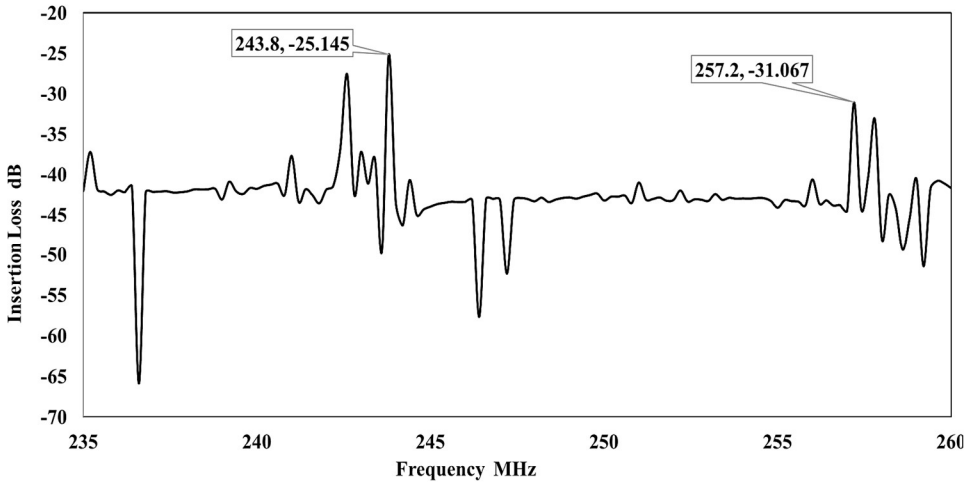


Figure 3. 12 Frequency Response [ 3D Model - Basic Structure]

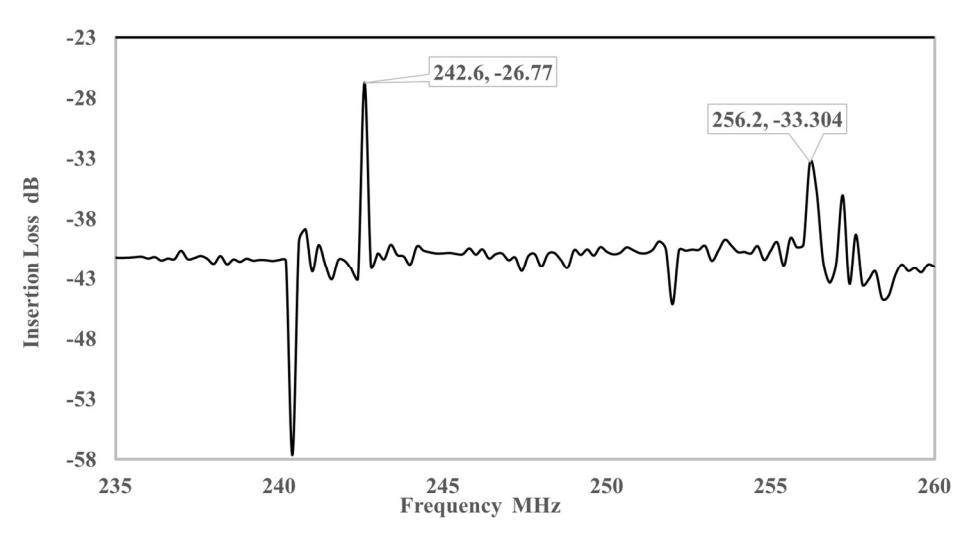


Figure 3. 13 Frequency Response with APTMS Protein Layer

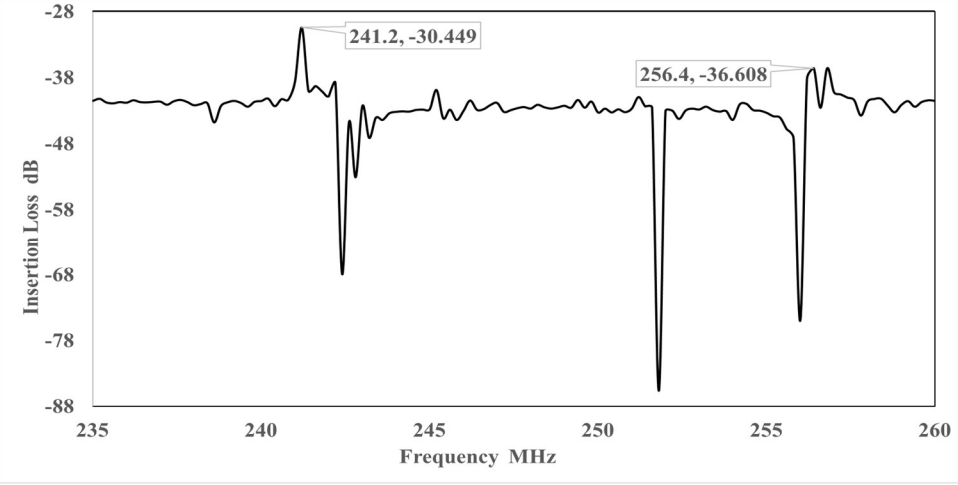


Figure 3. 14 Frequency Response with 5% SARS-CoV-2

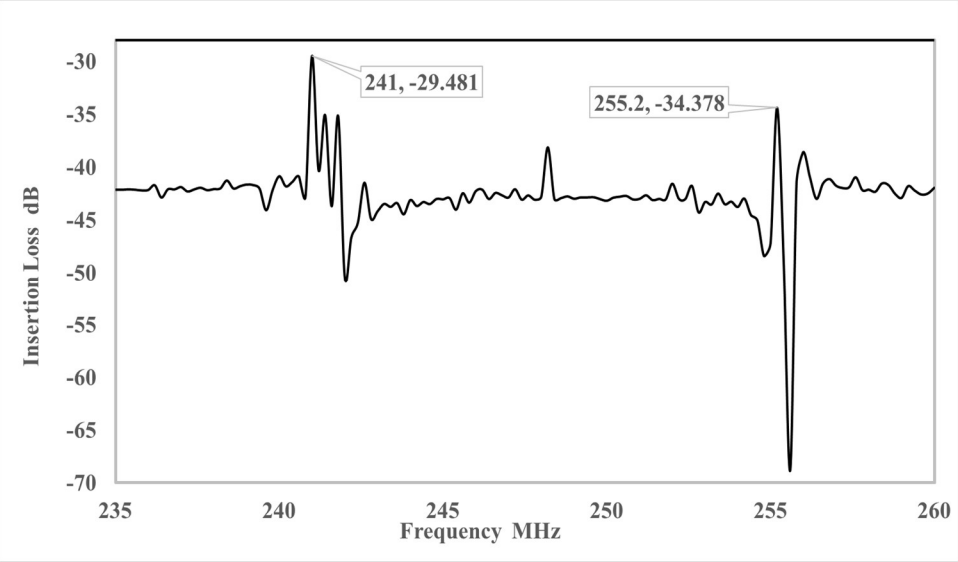


Figure 3. 15 Frequency Response with 30% SARS-CoV-2 Introduced To The Sensr Service

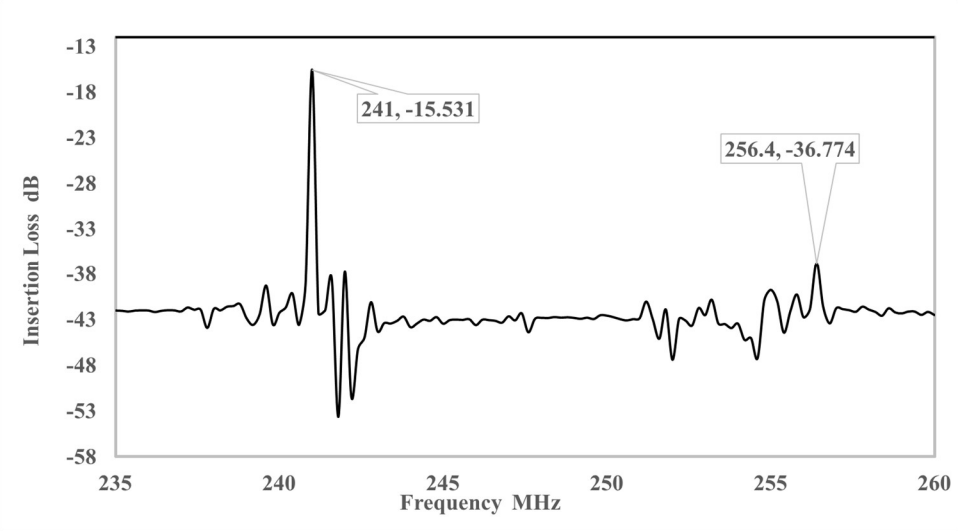


Figure 3. 16 Frequency Response with 83 % SARS-CoV-2

# CHAPTER FOUR
# SARS-COV-2 SPIKE ANTIBODY IMMOBILIZATION AND SARS-COV-2 CORONAVIRUSE DETECTION

## 4.1 Introduction

Developing extremely sensitive, chemically inert, and temperature-stable acoustic wave biosensor devices necessitates the development of novel and distinct material systems. In terms of surface acoustic wave biosensors, AlN (aluminum nitride) possesses a range of features that make it particularly well-suited. This material is piezoelectric and has significant piezoelectric coupling functionality, a linear temperature coefficient, high-temperature stability, and high thermal conductivity. So, the first step toward demonstrating a new method of attaching a biologically active layer to an AlN surface is to demonstrate whether molecules can be stabilized on AlN. This will pave the way for the selection and detection of environmental analytes, as well as their designation and monitoring.

In our study, a layer of silanes is formed from the solution onto the treated AlN surfaces by the chemical vapor deposition method in order to form chemical functional groups that will act as anchor sites for spike antibody of SARS -CoV-2.In addition, the adjustment of the density of macromolecule anchor points on the sensor surface by changing the percentage of silanes with a reactive end group in the composition of the silanes was conducted in this research.

The aluminum nitride surface is highly structured and has low surface energy. The surface is also quite hydrophobic. Various organic compounds and particles that are present in any open lab atmosphere will adsorb onto the AlN surface within minutes of

removing the film/wafer from the deposition chamber. These characteristics present difficulties when trying to form a covalent bond between the surface and another molecule. An important step in preparing an inorganic surface for salinization involves removing foreign materials from the surface and increasing the number of hydroxyl groups on the surface, which are known to participate in the bonding of the siloxane layer to the inorganic substrate.

The modification of AlN surfaces prior to salinization serves a dual function. One of the goals is to have a consistently clean surface immediately before the salinization process. Additionally, x-ray photoelectron spectroscopy (XPS) has shown that raw AlN surfaces have an additional layer of carbon-containing compounds adsorbed on the surface, in addition to the typical airborne tiny pollutants that would settle on the surface. This layer of adventitious carbon may be found on the majority of surfaces that are exposed to the surrounding environment. Another goal of surface treatment is to enhance the number of hydroxyl groups on the surface, which are thought to have a role in the anchoring of siloxane chains to the solid surface, as previously stated.

In order to immobilize SARS-CoV-2 (COVID-19) spike antibody on the AlN surface, a stable molecular layer was formed that serves as a link between the immobilizing agent/analyte conjugate and the film surface. This cross-linker layer was stable under the circumstances of sensor operation in order to function properly. Silanes are frequently used to derivatize inorganic surfaces, and they are very effective. When it comes to functional groups that constitute the surface of the cross-linker layer, there are many options accessible due to the large number of silanes that are commercially available. Salinization is well-known for producing very stable layers on various

substrates, and it has been widely investigated. As a result, salinization was chosen as the surface derivatization technique for this investigation.

APTMS is an amino silane that forms self-assembled monolayers (SAMs) on oxidized and/or hydroxylated surfaces when exposed to high temperatures. It is the methoxy (-$OCH_3$) part of the chemical that attaches to oxidized and/or hydroxylated surfaces, and it is this portion of the chemical that may create siloxane linkages with adjacent APTMS groups in a self-assembling manner. The amine end-group will be utilized to covalently attach and immobilize proteins to surfaces, usually in conjunction with another chemical (i.e., crosslinker).

The heterobifunctional crosslinkers 1-Ethyl-3-(3 dimethylaminopropyl)-carbodiimide (EDC) and sulfo-N-hydroxysuccinimide (Sulfo-NHS) will be used to immobilize covalently bound proteins on APTMS functionalized AlN surfaces for covalent protein immobilization. It is believed that EDC helps to enhance the binding of an amine to a carboxylic acid group (-COOH); carboxylic acids are found near the end of antibodies' FC regions in the form of glutamic or aspartic acid. Since protein orientation is more likely to occur when an antibody (Fab) is immobilized in the FC region, as opposed to random binding of lysines, NH2 groups, and other amino acid groups on the protein surface, the binding area of the antibody (Fab) may be made accessible for biological detection. Sulfo-NHS is a compound that helps in the stability of the EDC reaction.CVD (Chemical Vapor Deposition) is a chemical technique that is used to deposit layers with a variety of uses on a variety of surfaces. It is used in this deposition technique to expose the target surface (substrate) to a vaporized mixture of one or more chemicals. Then, in order to form a solid layer with the required chemical composition,

the gas atoms in the chamber disintegrate on the surface of the substrate or chemically react with one another in order to form a solid layer.

## 4.2 Real-Time Detection of SARS-CoV-2 (COVID-19) Experiment

### 4.2.1 Materials and Methods

The SH-SAW sensor was used for this experiment, as shown in Figure 4.1, and was fabricated in the SSIM clean room at Wayne State University. The biological and chemical materials used for this study are listed in Table 3.

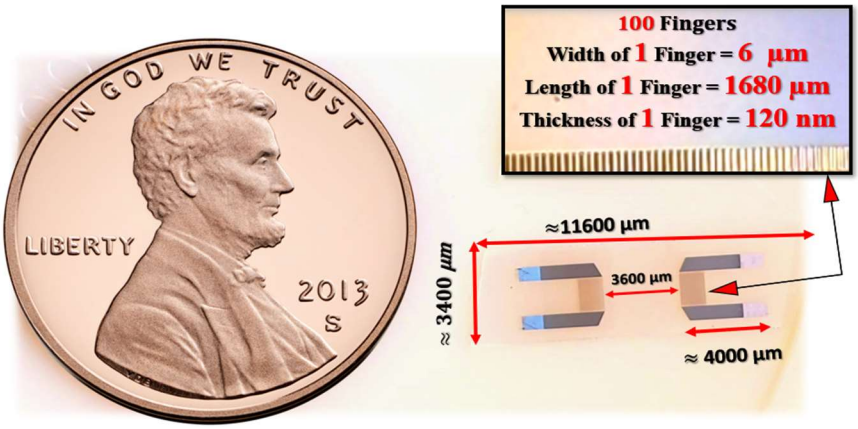


Figure 4. 1 The Fabricated SH-SAW Biosensor

Table 2 The list of the biological and chemicals materials

| Materials | Catalog number |
|---|---|
| 3-Aminopropyltrimethoxysilane (APTMS) | AC313251000 |
| EDC(1-ethyl-3-(3-dimethylaminopropyl) carbodiimide hydrochloride) | PG82079 |
| (EDC) Alternate | 77149 |
| N-Hydroxysulfosuccinimide (Sulfo-NHS) | PIA39269 |
| MES Buffer (pH 4.7) | PI28390 |
| PBS (pH 7.5) | AAJ62239AP |
| DMSO | BP231-100 |
| Tween-20 | AAJ61544AP |
| Recombinant SARS-CoV-2 (COVID-19) (S1) -1 Antibody | 0.1 mg (Alexa Fluor 532 conjugated) [CR3022] |
| SARS-CoV-2 | NR-52287, ATCC strain |
| Influenza B Yamagata | NR-36526, ATCC strain |
| The Human Coronavirus OC43 | - |

4.2.2.1 APTMS Chemical Vapor Deposition (CVD) on AlN

A Wheaton glass dry seal vacuum desiccator was used to deposit APTMS on AlN samples using CVD. AlN sample APTMS deposition was preceded by desiccator silanization through CVD. For 15 minutes, the samples were ultrasonically rinsed in water, acetone, and methanol. After that, nitrogen was used to dry the samples. Each sample was then placed AlN-face up in a clean glass container (with the sapphire side of the container touching). Then the desiccator lid was removed, and the vacuum was released. In the desiccator, 2-5 ml of APTMS were poured into the bottom, the metal plate was repositioned, the glass container containing the AlN samples was placed on top

of the metal plate, the desiccator lid was closed, and a vacuum of 14.2 psi was applied for 15 minutes before the vacuum was completely closed off, and the samples were left in the vacuumed environment for 16 hours. Afterward, the vacuum was released, and samples were rinsed in copious methanol and placed on an orbital shaker for 15–30 minutes twice before being dried with a stream of nitrogen. Desiccators were used to store samples that had been nitrogen-purged.

Five sample groups were introduced with the CVD deposition process, and each of them was provided with a different concentration of APTMS solutions, ranging from 3 mL to 5 mL. In addition, careful consideration was given to the amount of time that elapsed between the completion of the deposition by the CVD method and the beginning of the immobilization stage once the antibody was introduced into the samples.

#### 4.2.2.2 Immobilization of SARS-CoV-2 (COVID-19) Spike Antibody

There were different buffers prepared with the micro control solution. The solution containing 0.1M MES buffer was prepared by dissolving one pack in 500 mL of water; each pack made 0.1M MES, 0.9% sodium chloride, and pH 4.7. In Addition, DMSO buffer (1/2), (1-part Dimethyl Sulfoxide, 2 -parts deionized water) solution was prepared freshly, and (0.30% Tween-20) in MES buffer was prepared. The microchip solution, which includes SARS-CoV-2 Spike Antibody, was prepared and included 5 µg/mL SARS-CoV-2 Spike Antibody, 50 µl 18 mM Sulfo-NHS, 25 µl DMSO (1/2),420 µl, 0.30% Tween-20 in MES. Prepare 1 ml EDC solution. Finally, Introduce the SARS-CoV-2 Spike Antibody +EDC/MES solution to the two samples as follows:

a. Pipette 0.100 ml of the microchip solution that contains the spike antibodies.

b. Pipette 0.100 ml of the EDC solution into each well.

c. Incubate at room temperature with foil on top overnight.

4.2.2.3 Experiment for Selectivity & Sensitivity of SARS-CoV-2 Detection

Influenza B Yamagata and SARS-CoV-2 were employed in sample one, with a concentration of 2.0 x$10^6$ GE/ml and 1.2 x$10^6$ GE/ml, respectively. In order to reestablish the signal baseline for viral sensing, 10 and 25 microliters of sodium phosphate buffer solution (PBS) were introduced into the sensing area of sample 1. Following that, 10 and 25 microliters of an influenza B Yamagata virus strain containing a concentration of 2 x $10^6$ GE/ml were added, respectively, to sample 1. After that, PBS with Tween-20 was used for flushing the surface to eliminate unbound influenza. In addition to this, PBS was reintroduced in order to flush out the Tween-20, and the sensor was dried with nitrogen gas after each step. The identical processes were carried out for SARS-CoV-2 using a concentration of 1.2 x 106 GE/ml, and the result of the vectors Network Analyzer for the sample one frequency response was examined for both viruses.

Regarding the second sample, three different viruses were utilized in the testing and investigation of the performance of the sensor. The three viruses were Human Coronavirus OC43 virus, Influenza B Yamagata virus, and SARS-CoV-2. The Human Coronavirus OC43 virus had a concentration of 2x$10^6$ GE/ml, Influenza B Yamagata virus had a concentration of 2x$10^6$ GE/ml, and SARS-CoV-2 had a concentration of 1.2x$10^6$ GE/ml. In order to reestablish the signal baseline for viral detection, 5,10, and 15 µl of sodium phosphate buffer solution (PBS) were introduced into the sensing area at various points. After that, 5, 10, and 15 microliters of the Human Coronavirus OC43 virus were delivered into the sensing area of sample two. Afterward, PBS with Tween-20 was used for flushing the surface in order to eliminate any loosely bound influenza. PBS

was used once more to wash away the Tween-20, and nitrogen gas was used at each stage to completely dry the sensor. The same three methods have been carried out for the other viruses, which are Influenza B Yamagata and SARS-CoV-2, respectively.

## 4.3 Results of the Experiments

### 4.3.1 Raman Microscope for Antibody immobilization

An In Via Raman microscope (Renishaw, Gloucestershire, UK) equipped with a 514.5 nm excitation laser, 1800 l/mm grating, 576 x 400-pixel thermoelectric cooled charge-coupled device, and WiRE 3.4 software (Renishaw Inc., Hoffman Estates, IL) was used for Raman spectroscopic data acquisition. 5x and 50x N-plan Leica objectives (Leica Inc., Allendale, NJ) with a numeric aperture of 0.12 and 0.75, respectively, were used for the measurements. Spectra were measured at 50% laser power for one accumulation of 10 seconds each over the spectral range of 200 to 3200 $cm^{-1}$.

Recombinant SARS-CoV-2 (COVID-19) (S1) -1 Antibodies with Alexa Fluor 532 conjugated have been detected in two samples, as shown in Figures 4.2 and Figure 4.3. In addition, Figure 4.4 shows the results of the reference sample that doesn't have the antibody immobilized.

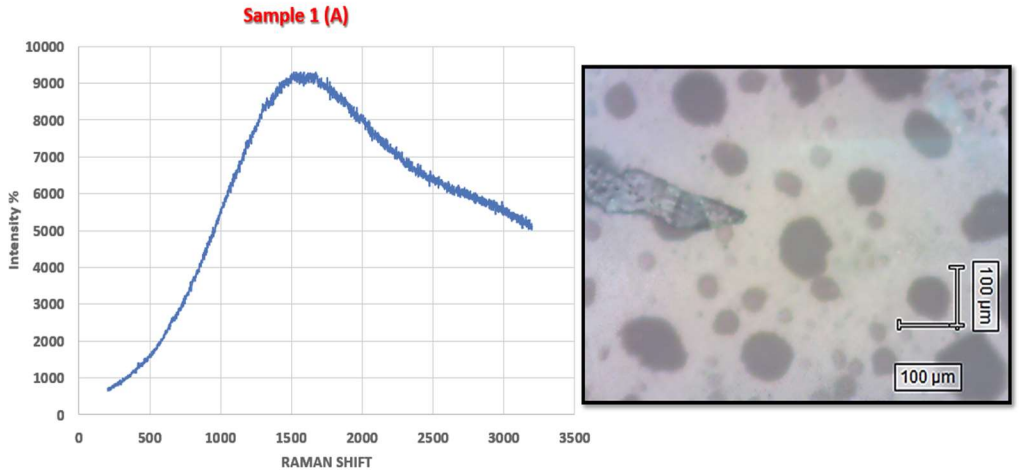


Figure 4. 2 Raman Microscope Results for Sample

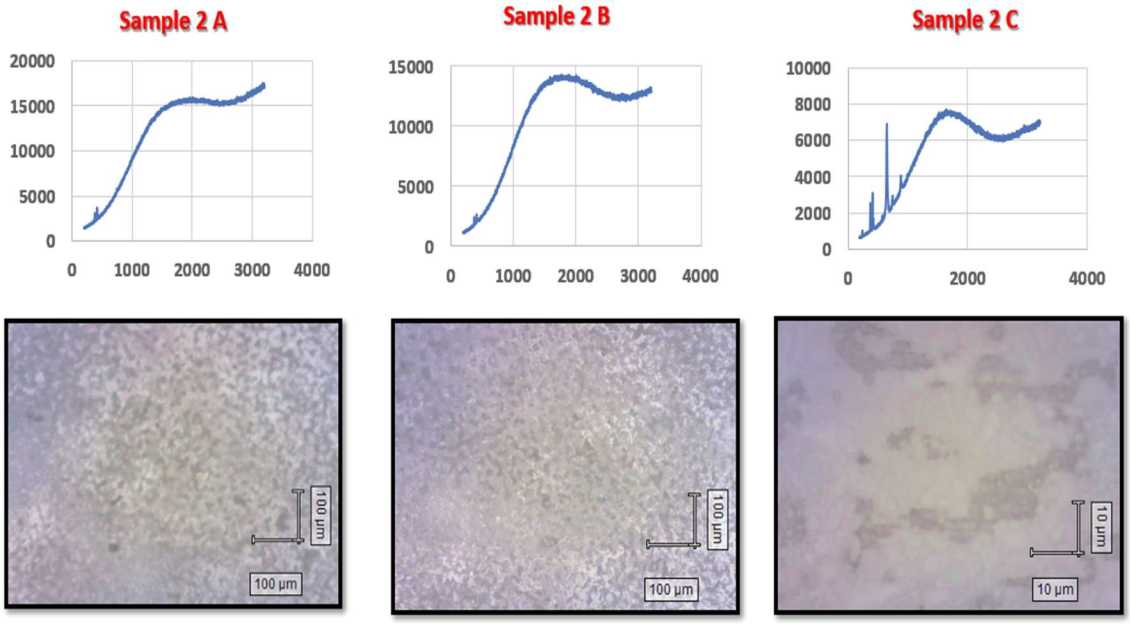


Figure 4. 3 Raman Microscope Results for Sample 2

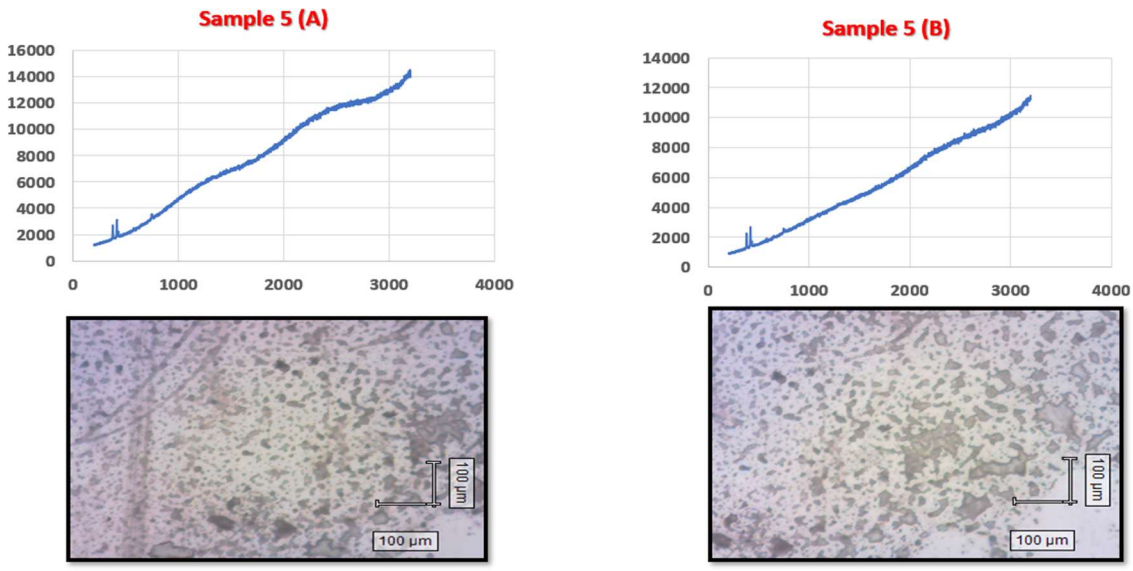


Figure 4. 4 Raman Microscope Results for Reference Sample

### 4.3.2 Biosensor Experiment for SARS-CoV-2 Detection

The velocity of the acoustic wave as it travels through the piezoelectric material is a significant factor in determining the resonance frequency of the SH-SAW sensor. It is well known that the wave's velocity shifts as a result of shifts in the mass, stiffness, conductivity, dielectric coefficient, temperature, and pressure of the medium. This resulted in a change in the resonant frequency, which can be used to confirm the binding between the spike antibodies and the increasing concentration or volume levels of viruses. This change in frequency can be used to confirm the binding between the spike antibodies and the increasing concentration levels of viruses.

After introducing different volumes and concentrations of SARS-CoV-2, Influenza B Yamagata, and Human Coronavirus OC43 to the surfaces of the two sensors, a network analyzer (HP 8753D) was used to measure the SH-SAW devices. The

differential volumes of SARS-CoV-2 that are delivered to the surface of the sensor induce a variation in the SAW propagation velocity between the input and output IDEs. This is because the virus binds to the spike antibodies that are immobilized in the APTMS protein sensing layer. However, after flashing the sensors with PBS, the frequency did not shift when Influenza B Yamagata and Human Coronavirus OC43 were introduced to both sensors.

For sample 1, it was determined that the resonant frequency that indicated the signal baseline of the PBS solution for SAW mode was 241.752 MHz, and that the frequency for SH-SAW mode was 254.294 MHz. Both of these values were found to be accurate. Additionally, the insertion losses of SAW and SH-SAW modes were, respectively, -26.92 dB and -30.563 dB. Concerning sample 2, it was found that the resonant frequency that indicated the signal baseline of the PBS solution for SAW mode was 240.50 MHz, and that the resonant frequency for SH-SAW mode was 253.536 MHz.

Regarding the frequency response of the SH-SAW sample 1 in relation to the saline solution that was introduced to the sensor surface as a baseline signal, it was noticed that the resonant frequency of the reference signal shifted for only SARS-CoV-2 in SAW mode, shifting from 241.752 MHz to 241.421 MHz for SARS-CoV-2 (10 µl ) and shifting from 241.752 MHz to 239.549 MHz for SARS-CoV-2 (25 µl). In addition to this, it was found that the resonant frequency of the reference signal shifted for SARS-CoV-2 (10 µl) in SH-SAW mode from 254.294 MHz to 254.036 MHz, and for SARS-CoV-2 (25 µl) from 254.036 MHz to 253.398 MHz. This phenomenon was observed for just SARS-CoV-2.

In regard to the insertion loss for sensor 1, it was observed that for only SARS-CoV-2, the insertion loss of the reference signal shifted for SAW mode for SARS-CoV-2 (10 µl) from -26.92 dB to -30.395 dB and shifted to -32.248 dB for SARS-CoV-2 (25 µl). These shifts were observed for only SARS-CoV-2. In addition to this, it was observed that the insertion loss of the reference signal changed for only SARS-CoV-2 in the SH-SAW mode for SARS-CoV-2 (10 µ) from -30.563 to -34.924 dB, and it shifted for SARS-CoV-2 (25 µl) to -32.87 dB.

Regarding the frequency response of sample 2 in relation to the saline solution that was introduced to the sensor surface as a baseline signal, it was observed for only SARS-CoV-2 that the resonant frequency shifted for both SAW and SH-SAW modes. The shift occurred for SARS-CoV-2 (5 µl) from 240.50 MHz to 237.84 MHz, for SARS-CoV-2 (10 µl) from 240.50 MHz to 238.16 MHz, and for SARS-CoV-2 (15 µl) from 240.50 MHz to 239.31.84 MHz. In addition, it was found that the resonant frequency of the reference signal shifted for SH-SAW mode for SARS-CoV-2 (5 µl) from 253.536 MHz to 253.922 MHz, for SARS-CoV-2 (10 µl) from 253.536 MHz to 254.607 MHz, and for SARS-CoV-2 (15 µl) from 253.536 MHz to 253.713 MHz.

In conclusion, with regard to the insertion loss for sensor 2, it was found that the insertion loss of the reference signal was shifted for SAW mode for only SARS-CoV-2, shifting from -29.100 dB to -30.645 dB for SARS-CoV-2 (5 µl), was shifting to -30.133 dB for SARS-CoV-2 (10 µl), and was shifting to -31.354 dB for SARS-CoV-2 (25 µl). Furthermore, it was shown that the insertion loss of the reference signal changed for SH-SAW mode for SARS-CoV-2 (5 µl) from -29.105 dB to -33.922 dB, for SARS-CoV-

2 (10 µl) was shifted to -33.629 dB, and for SARS-CoV-2 (15 µl) was shifted to -36.922 dB.

## 4.4 Discussion of the Experiments

In order to explore a new technique for applying biologically active molecules to the AlN surface to choose and detect environmental analytes of choice, the first job is intended to demonstrate a procedure for stabilizing these molecules on AlN. Salinization has been used as the primary technique of chemical derivatization for attaching the macromolecules to the inorganic AlN surface in this research since it is simple and effective. The inquiry is divided into three interconnected areas of investigation.

The surface evaluation of aluminum nitride surfaces was conducted. The AlN surfaces that have been "as-deposited" serve as the basis upon which the detecting surface is constructed. The characterization of these raw surfaces offers baseline data that may be used to compare the same surfaces after they have been modified. Aside from this, the characterization of these surfaces allows researchers to identify the differences between different AlN depositions in terms of composition, surface morphology, surface energy, and crystal structure.

Cleaning and treating AlN surfaces in preparation for salinization is a common practice. For the most part, it is accepted that the presence of hydroxyl groups is required for silane molecules to bind to a substrate surface. Surfaces of AlN materials are treated in order to produce these hydroxyl groups. Immersion in boiling water, exposure to ultraviolet radiation, immersion in a caustic solution, and exposure to plasma are just a few of the surface treatments now being investigated. Surface treatments are assessed by searching for negative effects on the AlN film (such as the loss of AlN material) and

changes in the surface hydroxyl groups, as measured by surface hydrophilicity, in order to determine if they are harmful.

With the use of silanes, aluminum nitride surfaces may be derivated. A layer of silanes is formed from the solution onto the treated AlN surfaces in order to form chemical functional groups that will act as anchor sites for proteins. The ability to salinize AlN using a single, well-studied silane is assessed by comparing the salinized AlN surfaces to a control that has not been salinized is investigated. In the next step, the AlN surfaces are salinized using a combination of two distinct silanes; one of the silanes has a reactive allyl end group, while the other contains a non-reactive methyl end group. It may be feasible to adjust the density of macromolecule anchor points on the sensor surface by changing the percentage of silanes with a reactive end group in the composition of the silanes.

# CHAPTER FIVE

# CONCLUSION AND FUTURE WORK

SARS-CoV-2 (coronavirus disease 2019) was the analyte of choice for this dissertation. SARS-CoV-2 (COVID-19) spike antibodies were immobilized by the immobilizing agent, which is attached to the sensor surface. The two sets of interdigital transducers (IDTs) that are produced on the surface of AlN transport electrical signals into or out of the AIN layer. When the signals are transduced into and out of the AlN film, acoustic waves travel throughout the sensing area. The spike antibodies were immobilized, and the changes in mass bound of SARS-CoV-2 to the surface were detected in the sensing region of our fabricated sensor.

COMSOL software was used for the design and modeling of the SH-SAW biosensor, and the simulated results agreed quite well with the experimentally measured values. These results support the design and show that the SAW mode is functional. The results of the simulation demonstrate the wave modes and how they propagate. The simulation findings are affected in various ways by the various reduced dimensions and material constants. The FEM analysis that was carried out in the process of this research provides a solid foundation that may be utilized in the future to minimize the amount of time required for the design of microelectromechanical systems and the cost of fabrication.

In order to detect SARS-CoV-2 (COVID-19) in real-time, the goal of this study was to identify a chemical linker that would enable the immobilization of spike antibodies on AlN surfaces while preserving its usefulness for protein detection. The

CVD procedures for APTMS on AlN were investigated in order to immobilize the spark antibody, which was then used for antibody immobilization. The findings revealed that the AlN passivation oxygen layer that formed in order to close the lattice after the AlN was withdrawn from the PSMBE chamber was appropriate for the CVD deposition of APTMS in order to generate a monolayer or near-monolayer surfaces. The APTMS-modified AlN surfaces served as a platform for the covalent immobilization of complex organics (antibodies) to the otherwise inert AlN surface. This was made possible because of the immobilization of complex organics by the APTMS. Because of the use of the crosslinkers EDC and Sulfo-NHS, it was possible to achieve covalent immobilization between the amines on the APTMS coated surface and the carboxylic acids on the antibodies in the FC region. As a result, the results indicated that the antibodies were relatively oriented and that they maintained their functionality after being immobilized. The immobilized antibodies made it possible to carry out virus detection in a particularly targeted manner.

In order to verify that antibodies were successfully immobilized onto amino-silanized AlN surfaces, Raman microscopy was performed. In the research that we did, we found that covalent alteration led to increased detection. It was a helpful piece of qualitative equipment. It was helpful in seeing various protein-APTMS coated surfaces as well as protein-protein interactions. The use of methods involving covalent binding was validated by this approach of characterization. Detecting viruses with covalently immobilized antibodies that presented affinity resulted in specific binding; however, when testing with antibodies that did not provide affinity or bacteria, no binding was found utilizing the Network Analyzer test.

For examining the sensitivity and selectivity of our SH-SAW biosensor, SARS-CoV-2, Influenza B Yamagata, and Human Coronavirus OC43 were all applied to the surfaces of the two sensors, and the devices were then analyzed by a network analyzer (HP 8753D). The interaction between the virus and the spike antibody immobilized in the APTMS protein sensing layer causes a shift in the SAW propagation velocity between the input and output IDEs when different volumes and concentrations of SARS-CoV-2 are delivered to the sensor surface. Both sensors showed no change in frequency after being exposed to Influenza A Yamagata and Human Coronavirus OC43.

Finally, despite encouraging results, further sensor analysis is needed for testing APTMS through CVD on a SAW sensor. Chemical deposition and antibody immobilization components of APTMS must be examined using AFM and other accessible techniques. The detection system must be quantified because the ultimate goal is to package the AW sensor system into a portable, hand-held device. All components must be addressed and quantified. APTMS-modified AlN surfaces may be worked on while the sensor system is being completed. What comes after this is important: Analysis of AlN surfaces before and after APTMS depositions, and immobilization and assessment of the antibodies investigated and additional antibodies.

# Reference


[1] T. P. Velavan and C. G. Meyer, "The COVID-19 epidemic," *Tropical Medicine & International Health*, vol. 25, no. 3, p. 278, Mar. 2020, doi: 10.1111/TMI.13383.

[2] S. Khan *et al.*, "Coronavirus diseases 2019: Current biological situation and potential therapeutic perspective," *European Journal of Pharmacology*, vol. 886, no. July, p. 173447, 2020, doi: 10.1016/j.ejphar.2020.173447.

[3] M. Asif *et al.*, "The role of biosensors in coronavirus disease-2019 outbreak," *Current Opinion in Electrochemistry*, vol. 23, pp. 174–184, Oct. 2020, doi: 10.1016/J.COELEC.2020.08.011.

[4] Y. Shen, T. bin Anwar, and A. Mulchandani, "Current status, advances, challenges and perspectives on biosensors for COVID-19 diagnosis in resource-limited settings," *Sensors and Actuators Reports*, vol. 3, no. January, p. 100025, 2021, doi: 10.1016/j.snr.2021.100025.

[5] F. Narita *et al.*, "A Review of Piezoelectric and Magnetostrictive Biosensor Materials for Detection of COVID-19 and Other Viruses," *Advanced Materials*, vol. 33, no. 1, 2021, doi: 10.1002/adma.202005448.

[6] N. Bhalla, P. Jolly, N. Formisano, and P. Estrela, "Introduction to biosensors," *Essays in Biochemistry*, pp. 60–61, 2016, doi: 10.1042/EBC20150001.

[7] Z. Rezaei and M. Mahmoudifard, "Pivotal role of electrospun nanofibers in microfluidic diagnostic systems-a review," *Journal of Materials Chemistry B*, vol. 7, no. 30. Royal Society of Chemistry, pp. 4602–4619, Jul. 31, 2019. doi: 10.1039/c9tb00682f.

[8] E. Morales-Narváez and C. Dincer, "The impact of biosensing in a pandemic outbreak: COVID-19," *Biosensors and Bioelectronics*, vol. 163, p. 112274, Sep. 2020, doi: 10.1016/J.BIOS.2020.112274.

[9] I. H. Cho *et al.*, "Nano/micro and spectroscopic approaches to food pathogen detection," *Annual Review of Analytical Chemistry*, vol. 7. 2014. doi: 10.1146/annurev-anchem-071213-020249.

[10] Y. Lyu, D. Cui, J. Huang, W. Fan, Y. Miao, and K. Pu, "Near-Infrared Afterglow Semiconducting Nano-Polycomplexes for the Multiplex Differentiation of Cancer Exosomes," *Angewandte Chemie - International Edition*, vol. 58, no. 15, pp. 4983–4987, Apr. 2019, doi: 10.1002/anie.201900092.

[11] A. Afzal, A. Mujahid, R. Schirhagl, S. Z. Bajwa, U. Latif, and S. Feroz, "Gravimetric viral diagnostics: QCM based biosensors for early detection of viruses," *Chemosensors*, vol. 5, no. 1. MDPI Multidisciplinary Digital Publishing Institute, p. 7, Mar. 01, 2017. doi: 10.3390/chemosensors5010007.

[12] A. D. Chowdhury, K. Takemura, T. C. Li, T. Suzuki, and E. Y. Park, "Electrical pulse-induced electrochemical biosensor for hepatitis E virus detection," *Nature Communications*, vol. 10, no. 1, pp. 1–12, Dec. 2019, doi: 10.1038/s41467-019-11644-5.

[13] T. Ji *et al.*, "Detection of COVID-19: A review of the current literature and future perspectives," *Biosensors and Bioelectronics*, vol. 166, no. July, p. 112455, 2020, doi: 10.1016/j.bios.2020.112455.

[14] A. C. Walls, Y. J. Park, M. A. Tortorici, A. Wall, A. T. McGuire, and D. Veesler, "Structure, Function, and Antigenicity of the SARS-CoV-2 Spike Glycoprotein," *Cell*, vol. 181, no. 2, pp. 281-292.e6, 2020, doi: 10.1016/j.cell.2020.02.058.

[15] D. Wrapp *et al.*, "Cryo-EM Structure of the 2019-nCoV Spike in the Prefusion Conformation.," *bioRxiv*, Feb. 2020, doi: 10.1101/2020.02.11.944462.

[16] K. K. Lum and I. M. Cristea, "Proteomic approaches to uncovering virus-host protein interactions during the progression of viral infection," *Expert Review of Proteomics*, vol. 13, no. 3. Taylor and Francis Ltd, pp. 325–340, Mar. 03, 2016. doi: 10.1586/14789450.2016.1147353.

[17] E. Skarstein Kolberg, "ACE2, COVID19 and serum ACE as a possible biomarker to predict severity of disease," *Journal of Clinical Virology*, vol. 126. Elsevier B.V., May 01, 2020. doi: 10.1016/j.jcv.2020.104350.

[18] M. Hoffmann *et al.*, "SARS-CoV-2 Cell Entry Depends on ACE2 and TMPRSS2 and Is Blocked by a Clinically Proven Protease Inhibitor," *Cell*, vol. 181, no. 2, pp. 271-280.e8, Apr. 2020, doi: 10.1016/j.cell.2020.02.052.

[19] S. M. Russell, A. Alba-Patiño, E. Barón, M. Borges, M. Gonzalez-Freire, and R. de La Rica, "Biosensors for Managing the COVID-19 Cytokine Storm: Challenges Ahead," *ACS Sensors*, vol. 5, no. 6, pp. 1506–1513, Jun. 2020, doi: 10.1021/acssensors.0c00979.

[20] H. Zhu, Z. Fohlerová, J. Pekárek, E. Basova, and P. Neužil, "Recent advances in lab-on-a-chip technologies for viral diagnosis," *Biosensors and Bioelectronics*, vol. 153. Elsevier Ltd, Apr. 01, 2020. doi: 10.1016/j.bios.2020.112041.

[21] J. J. Waggoner *et al.*, "Triplex Real-Time RT-PCR for Severe Acute Respiratory Syndrome Coronavirus 2," *Emerging Infectious Diseases*, vol. 26, no. 7, pp. 1633–1635, Jul. 2020, doi: 10.3201/eid2607.201285.

[22] M. M. Ngundi, N. v. Kulagina, G. P. Anderson, and C. R. Taitt, "Nonantibody-based recognition: Alternative molecules for detection of pathogens," *Expert Review of Proteomics*, vol. 3, no. 5. Taylor & Francis, pp. 511–524, 2006. doi: 10.1586/14789450.3.5.511.

[23] B. Zuo, S. Li, Z. Guo, J. Zhang, and C. Chen, "Piezoelectric immunosensor for SARS-associated coronavirus in sputum," *Analytical Chemistry*, vol. 76, no. 13, pp. 3536–3540, Jul. 2004, doi: 10.1021/ac035367b.

[24] T. M. Peduru Hewa, G. A. Tannock, D. E. Mainwaring, S. Harrison, and J. v. Fecondo, "The detection of influenza A and B viruses in clinical specimens using a quartz crystal microbalance," *Journal of Virological Methods*, vol. 162, no. 1, p. 14, Jan. 2009, doi: 10.1016/J.JVIROMET.2009.07.001.

[25] H. Zhang and B. L. Miller, "Immunosensor-based label-free and multiplex detection of influenza viruses: State of the art," *Biosensors and Bioelectronics*, vol. 141. Elsevier Ltd, Sep. 15, 2019. doi: 10.1016/j.bios.2019.111476.

[26] L. M. Pandey and S. K. Pattanayek, "Hybrid surface from self-assembled layer and its effect on protein adsorption," *Applied Surface Science*, vol. 257, no. 10, pp. 4731–4737, Mar. 2011, doi: 10.1016/j.apsusc.2010.12.148.

[27] T. Deng *et al.*, "Quartz crystal microbalance bioaffinity sensor for biotin based on mixed self-assembled monolayers and metastable molecular complex receptor," *Biosensors and Bioelectronics*, vol. 21, no. 8, pp. 1545–1552, Feb. 2006, doi: 10.1016/j.bios.2005.07.001.

[28] V. C. C. Cheng, S. K. P. Lau, P. C. Y. Woo, and Y. Y. Kwok, "Severe acute respiratory syndrome coronavirus as an agent of emerging and reemerging infection," *Clinical Microbiology Reviews*, vol. 20, no. 4. 2007. doi: 10.1128/CMR.00023-07.

[29] M. P. Girard, J. S. Tam, O. M. Assossou, and M. P. Kieny, "The 2009 A (H1N1) influenza virus pandemic: A review," *Vaccine*, vol. 28, no. 31. 2010. doi: 10.1016/j.vaccine.2010.05.031.

[30] A. Zumla, D. S. Hui, and S. Perlman, "Middle East respiratory syndrome," *The Lancet*, vol. 386, pp. 995–1007, 2015, doi: 10.1016/S0140-6736(15)60454-8.

[31] O. O. Oleribe *et al.*, “Ebola virus disease epidemic in West Africa: Lessons learned and issues arising from West African countries,” *Clinical Medicine, Journal of the Royal College of Physicians of London*, vol. 15, no. 1, 2015, doi: 10.7861/clinmedicine.15-1-54.

[32] M. Atif, M. Azeem, M. R. Sarwar, and A. Bashir, “Zika virus disease: a current review of the literature,” *Infection*, vol. 44, no. 6. 2016. doi: 10.1007/s15010-016-0935-6.

[33] B. U. Yildiz, K. Yanik, and O. Yakupoğlu, “Zika virus: A current review of literature,” *University of Toronto Medical Journal*, vol. 96, no. 3. 2019.

[34] Z. W. Ye, S. Yuan, K. S. Yuen, S. Y. Fung, C. P. Chan, and D. Y. Jin, “Zoonotic origins of human coronaviruses,” *International Journal of Biological Sciences*, vol. 16, no. 10. 2020. doi: 10.7150/ijbs.45472.

[35] B. Alhalaili, I. N. Popescu, O. Kamoun, F. Alzubi, S. Alawadhia, and R. Vidu, “Nanobiosensors for the detection of novel coronavirus 2019-ncov and other pandemic/epidemic respiratory viruses: A review,” *Sensors (Switzerland)*, vol. 20, no. 22. 2020. doi: 10.3390/s20226591.

[36] R. J. G. Hulswit, C. A. M. de Haan, and B. J. Bosch, “Coronavirus Spike Protein and Tropism Changes,” in *Advances in Virus Research*, vol. 96, 2016. doi: 10.1016/bs.aivir.2016.08.004.

[37] R. Gorkhali, P. Koirala, S. Rijal, A. Mainali, A. Baral, and H. K. Bhattarai, “Structure and Function of Major SARS-CoV-2 and SARS-CoV Proteins,” *Bioinformatics and Biology Insights*, vol. 15. 2021. doi: 10.1177/11779322211025876.

[38] M. A. C. Huergo and N. T. K. Thanh, “Current advances in the detection of COVID-19 and evaluation of the humoral response,” *Analyst*, vol. 146, no. 2, pp. 382–402, 2021, doi: 10.1039/d0an01686a.

[39] W. H. Sheng, *Coronavirus disease 2019 (covid-19)*, vol. 31, no. 2. 2020. doi: 10.6314/JIMT.202004_31(2).01.

[40] S. Satarker and M. Nampoothiri, “Structural Proteins in Severe Acute Respiratory Syndrome Coronavirus-2,” *Archives of Medical Research*, vol. 51, no. 6. 2020. doi: 10.1016/j.arcmed.2020.05.012.

[41] B. Boson *et al.*, “The SARS-CoV-2 envelope and membrane proteins modulate maturation and retention of the spike protein, allowing assembly of virus-like particles,” *Journal of Biological Chemistry*, vol. 296, 2021, doi: 10.1074/jbc.RA120.016175.

[42] A. C. Walls, Y. J. Park, M. A. Tortorici, A. Wall, A. T. McGuire, and D. Veesler, "Structure, Function, and Antigenicity of the SARS-CoV-2 Spike Glycoprotein," *Cell*, vol. 181, no. 2, pp. 281-292.e6, Apr. 2020, doi: 10.1016/j.cell.2020.02.058.

[43] L. M. Pandey, "Design of engineered surfaces for prospective detection of Sars-CoV-2 using quartz crystal microbalance based techniques," *Expert Review of Proteomics*, 2020, doi: 10.1080/14789450.2020.1794831.

[44] Y. Chen, Y. Guo, Y. Pan, and Z. J. Zhao, "Structure analysis of the receptor binding of 2019-nCoV," *Biochemical and Biophysical Research Communications*, vol. 525, no. 1, pp. 135–140, Apr. 2020, doi: 10.1016/j.bbrc.2020.02.071.

[45] Q. Han, Q. Lin, S. Jin, and L. You, "Coronavirus 2019-nCoV: A brief perspective from the front line," *Journal of Infection*, vol. 80, no. 4, pp. 373–377, 2020, doi: 10.1016/j.jinf.2020.02.010.

[46] L. Xu, D. Li, S. Ramadan, Y. Li, and N. Klein, "Facile biosensors for rapid detection of COVID-19," *Biosensors and Bioelectronics*, vol. 170, Dec. 2020, doi: 10.1016/j.bios.2020.112673.

[47] F. Cui and H. S. Zhou, "Diagnostic methods and potential portable biosensors for coronavirus disease 2019," *Biosensors and Bioelectronics*, vol. 165, no. June, p. 112349, 2020, doi: 10.1016/j.bios.2020.112349.

[48] D. K. W. Chu *et al.*, "Molecular Diagnosis of a Novel Coronavirus (2019-nCoV) Causing an Outbreak of Pneumonia," *Clin Chem*, vol. 66, no. 4, pp. 549–555, Apr. 2020, doi: 10.1093/clinchem/hvaa029.

[49] H. X. Bai *et al.*, "Performance of Radiologists in Differentiating COVID-19 from Non-COVID-19 Viral Pneumonia at Chest CT," *Radiology*, vol. 296, no. 2, 2020, doi: 10.1148/radiol.2020200823.

[50] L. Li *et al.*, "Using Artificial Intelligence to Detect COVID-19 and Community-acquired Pneumonia Based on Pulmonary CT: Evaluation of the Diagnostic Accuracy," *Radiology*, vol. 296, no. 2, 2020, doi: 10.1148/radiol.2020200905.

[51] S. Zhou, Y. Wang, T. Zhu, and L. Xia, "CT features of coronavirus disease 2019 (COVID-19) pneumonia in 62 patients in Wuhan, China," *American Journal of Roentgenology*, vol. 214, no. 6, 2020, doi: 10.2214/AJR.20.22975.

[52] L. Zou *et al.*, "SARS-CoV-2 Viral Load in Upper Respiratory Specimens of Infected Patients," *New England Journal of Medicine*, vol. 382, no. 12, pp. 1177–1179, Mar. 2020, doi: 10.1056/NEJMC2001737.

[53] M. Asif *et al.*, “The role of biosensors in coronavirus disease-2019 outbreak,” *Current Opinion in Electrochemistry*, vol. 23, pp. 174–184, Oct. 2020, doi: 10.1016/J.COELEC.2020.08.011.

[54] T. C. Jackson, B. O. Patani, and D. E. Ekpa, “Nanotechnology in Diagnosis: A Review,” *Advances in Nanoparticles*, vol. 06, no. 03, 2017, doi: 10.4236/anp.2017.63008.

[55] G. Palestino, I. García-Silva, O. González-Ortega, and S. Rosales-Mendoza, “Can nanotechnology help in the fight against COVID-19?,” *Expert Review of Anti-Infective Therapy*, vol. 18, no. 9, pp. 849–864, 2020, doi: 10.1080/14787210.2020.1776115.

[56] G. Rocchitta *et al.*, “Enzyme biosensors for biomedical applications: Strategies for safeguarding analytical performances in biological fluids,” *Sensors (Switzerland)*, vol. 16, no. 6. 2016. doi: 10.3390/s16060780.

[57] V. M. Corman *et al.*, “Detection of 2019 novel coronavirus (2019-nCoV) by real-time RT-PCR,” *Eurosurveillance*, vol. 25, no. 3, p. 2000045, Jan. 2020, doi: 10.2807/1560-7917.ES.2020.25.3.2000045.

[58] J. Won *et al.*, “Development of a laboratory-safe and low-cost detection protocol for SARS-CoV-2 of the Coronavirus Disease 2019 (COVID-19),” *Experimental Neurobiology*, vol. 29, no. 2, pp. 107–119, Apr. 2020, doi: 10.5607/en20009.

[59] M. Y. Chan *et al.*, “The risks of ubiquinone and β-carotene deficiency and metabolic disorders in patients with oral cancer,” *BMC Cancer*, vol. 20, no. 1, Apr. 2020, doi: 10.1186/s12885-020-06839-9.

[60] A. Wu *et al.*, “Genome Composition and Divergence of the Novel Coronavirus (2019-nCoV) Originating in China,” *Cell Host and Microbe*, vol. 27, no. 3, pp. 325–328, Mar. 2020, doi: 10.1016/j.chom.2020.02.001.

[61] P. C. Y. Woo *et al.*, “Differential sensitivities of severe acute respiratory syndrome (SARS) coronavirus spike polypeptide enzyme-linked immunosorbent assay (ELISA) and SARS coronavirus nucleocapsid protein ELISA for serodiagnosis of SARS coronavirus pneumonia,” *Journal of Clinical Microbiology*, vol. 43, no. 7, pp. 3054–3058, Jul. 2005, doi: 10.1128/JCM.43.7.3054-3058.2005.

[62] H. Jiang *et al.*, “Global profiling of SARS-CoV-2 specific IgG/ IgM responses of convalescents using a proteome microarray,” *Nature Communications*, p. 2020.03.20.20039495, Mar. 2020, doi: 10.1101/2020.03.20.20039495.

[63] K. K. W. To *et al.*, “Saliva as a diagnostic specimen for testing respiratory virus by a point-of-care molecular assay: a diagnostic validity study,” *Clinical Microbiology and Infection*, vol. 25, no. 3, pp. 372–378, Mar. 2019, doi: 10.1016/j.cmi.2018.06.009.

[64] H. Pan, Z. Zhang, Q. Cao, X. Wang, and Z. Lin, “Conditional assessment of large-scale infrastructure systems using deep learning approaches (Conference Presentation),” Apr. 2020, vol. 11382, p. 28. doi: 10.1117/12.2560133.

[65] Y. Pan *et al.*, “Serological immunochromatographic approach in diagnosis with SARS-CoV-2 infected COVID-19 patients,” *Journal of Infection*, vol. 81, no. 1, pp. e28–e32, Jul. 2020, doi: 10.1016/j.jinf.2020.03.051.

[66] D. S. Ballantine *et al.*, “Chemical and Biological Sensors,” *Acoustic Wave Sensors*, pp. 222–330, Jan. 1997, doi: 10.1016/B978-012077460-9/50005-8.

[67] R. L. Bunde, E. J. Jarvi, and J. J. Rosentreter, “Piezoelectric quartz crystal biosensors,” *Talanta*, vol. 46, no. 6, pp. 1223–1236, Aug. 1998, doi: 10.1016/S0039-9140(97)00392-5.

[68] D. A. Giljohann and C. A. Mirkin, “Drivers of biodiagnostic development,” 2009, doi: 10.1038/nature08605.

[69] Y. Huang, P. K. Das, and V. R. Bhethanabotla, “Surface acoustic waves in biosensing applications,” *Sensors and Actuators Reports*, vol. 3, 2021, doi: 10.1016/j.snr.2021.100041.

[70] M.-I. Rocha-Gaso, C. March-Iborra, Á. Montoya-Baides, and A. Arnau-Vives, “Surface Generated Acoustic Wave Biosensors for the Detection of Pathogens: A Review,” *Sensors*, vol. 9, no. 7, 2009, doi: 10.3390/s90705740.

[71] A. Mujahid, A. Afzal, and F. L. Dickert, “An overview of high frequency acoustic sensors—QCMs, SAWs and FBARs—chemical and biochemical applications,” *Sensors (Switzerland)*, vol. 19, no. 20. 2019. doi: 10.3390/s19204395.

[72] K. Länge, “Bulk and surface acoustic wave sensor arrays for multi-analyte detection: A review,” *Sensors (Switzerland)*, vol. 19, no. 24, 2019, doi: 10.3390/s19245382.

[73] S. Li and V. R. Bhethanabotla, “Design of a portable orthogonal surface acoustic wave sensor system for simultaneous sensing and removal of nonspecifically bound proteins,” *Sensors (Switzerland)*, vol. 19, no. 18, 2019, doi: 10.3390/s19183876.

[74] H. J. Lee, S. S. Lee, K. Namkoong, C. Ko, and J. C. Park, “SAW immunosensors for HBsAb detection,” *Proceedings of IEEE Sensors*, pp. 231–234, 2008, doi: 10.1109/ICSENS.2008.4716423.

[75] A. Mujahid and F. L. Dickert, “Surface acousticwave (SAW) for chemical sensing applications of recognition layers,” *Sensors (Switzerland)*, vol. 17, no. 12. 2017. doi: 10.3390/s17122716.

[76] F. di Pietrantonio *et al.*, “A surface acoustic wave bio-electronic nose for detection of volatile odorant molecules,” *Biosensors and Bioelectronics*, vol. 67, pp. 516–523, May 2015, doi: 10.1016/J.BIOS.2014.09.027.

[77] N. H. Hasanuddin *et al.*, “Design and Development of ZnO Based Gas Sensor for Fruit Ripening Detection,” in *MATEC Web of Conferences*, 2016, vol. 78. doi: 10.1051/matecconf/20167801109.

[78] J. Devkota, P. R. Ohodnicki, D. W. Greve, J. Luo, W. Xuan, and R. Y. Q. Fu, “SAW Sensors for Chemical Vapors and Gases”, doi: 10.3390/s17040801.

[79] T. J. Lyford, P. J. Millard, and M. P. da Cunha, “Cell lysisa using surface acoustic wave devices for sensor applications,” 2012. doi: 10.1109/ULTSYM.2012.0303.

[80] D. Taller *et al.*, “On-chip surface acoustic wave lysis and ion-exchange nanomembrane detection of exosomal RNA for pancreatic cancer study and diagnosis,” *Lab on a Chip*, vol. 15, no. 7, 2015, doi: 10.1039/c5lc00036j.

[81] J. Reboud *et al.*, “Shaping acoustic fields as a toolset for microfluidic manipulations in diagnostic technologies,” *Proc Natl Acad Sci U S A*, vol. 109, no. 38, 2012, doi: 10.1073/pnas.1206055109.

[82] C. Gao, S. Peng, P. Feng, and C. Shuai, “Bone biomaterials and interactions with stem cells,” *Bone Research*, vol. 5. 2017. doi: 10.1038/boneres.2017.59.

[83] S. A. Hunter and J. R. Cochran, “Cell-Binding Assays for Determining the Affinity of Protein–Protein Interactions: Technologies and Considerations,” *Methods in Enzymology*, vol. 580, pp. 21–44, Jan. 2016, doi: 10.1016/BS.MIE.2016.05.002.

[84] F. Klumpers, U. Götz, T. Kurtz, C. Herrmann, and T. M. A. Gronewold, “Conformational changes at protein–protein interaction followed online with an SAW biosensor,” *Sensors and Actuators B: Chemical*, vol. 203, pp. 904–908, Nov. 2014, doi: 10.1016/J.SNB.2014.07.064.

[85] M. Saitakis, A. Dellaporta, and E. Gizeli, “Measurement of Two-Dimensional Binding Constants between Cell-Bound Major Histocompatibility Complex and Immobilized Antibodies with an Acoustic Biosensor,” *Biophysical Journal*, vol. 95, no. 10, pp. 4963–4971, Nov. 2008, doi: 10.1529/BIOPHYSJ.108.132118.

[86] J. E. Roederer and G. J. Bastiaans, “Microgravimetric Immunoassay with Piezoelectric Crystals,” *Analytical Chemistry*, vol. 55, no. 14, 1983, doi: 10.1021/ac00264a030.

[87] W. Welsch, C. Kleln, M. von Schickfus, and S. Hunklinger, “Development of a surface acoustic wave immunosensor,” *Analytical Chemistry*, vol. 68, no. 13, 1996, doi: 10.1021/ac960198z.

[88] D. Mandal and S. Banerjee, “Surface AcousticWave (SAW) Sensors: Physics, Materials, and Applications,” *Sensors*, vol. 22, no. 3, 2022, doi: 10.3390/s22030820.

[89] S. Sharma, H. Byrne, and R. J. O’Kennedy, “Antibodies and antibody-derived analytical biosensors,” *Essays in Biochemistry*, vol. 60, no. 1, 2016, doi: 10.1042/EBC20150002.

[90] N. G. Welch, J. A. Scoble, B. W. Muir, and P. J. Pigram, “Orientation and characterization of immobilized antibodies for improved immunoassays (Review),” *Biointerphases*, vol. 12, no. 2, p. 02D301, 2017, doi: 10.1116/1.4978435.

[91] F. W. Scheller, “Vladimir M. Mirsky (Ed.): Ultrathin Electrochemical Chemo- and Biosensors: Technology and Performance,” *Analytical and Bioanalytical Chemistry*, vol. 386, no. 2, 2006, doi: 10.1007/s00216-006-0536-9.

[92] A. K. Trilling, J. Beekwilder, and H. Zuilhof, “Antibody orientation on biosensor surfaces: A minireview,” *Analyst*, vol. 138, no. 6. 2013. doi: 10.1039/c2an36787d.

[93] M. Shen, J. F. Rusling, and C. K. Dixit, “Site-selective orientated immobilization of antibodies and conjugates for immunodiagnostics development,” *Methods*, vol. 116, pp. 95–111, 2017, doi: 10.1016/j.ymeth.2016.11.010.

[94] P. J. Conroy, S. Hearty, P. Leonard, and R. J. O’Kennedy, “Antibody production, design and use for biosensor-based applications,” *Seminars in Cell and Developmental Biology*, vol. 20, no. 1. 2009. doi: 10.1016/j.semcdb.2009.01.010.

[95] D. Kim and A. E. Herr, “Protein immobilization techniques for microfluidic assays,” *Biomicrofluidics*, vol. 7, no. 4, 2013, doi: 10.1063/1.4816934.

[96] *Handbook of Biosensors and Biochips*. 2008. doi: 10.1002/9780470061565.

[97] T. Vo-Dinh and B. Cullum, "Biosensors and biochips: Advances in biological and medical diagnostics," *Fresenius' Journal of Analytical Chemistry*, vol. 366, no. 6–7. 2000. doi: 10.1007/s002160051549.

[98] D. Samanta and A. Sarkar, "Immobilization of bio-macromolecules on self-assembled monolayers: Methods and sensor applications," *Chemical Society Reviews*, vol. 40, no. 5, 2011, doi: 10.1039/c0cs00056f.

[99] M. Zourob, *Recognition receptors in biosensors*. 2010. doi: 10.1007/978-1-4419-0919-0.

[100] C. Campbell and J. C. Burgess, "Surface Acoustic Wave Devices and Their Signal Processing Applications," *J Acoust Soc Am*, vol. 89, no. 3, 1991, doi: 10.1121/1.400569.

[101] K. Hashimoto, *Surface Acoustic Wave Devices in Telecommunications*. 2000. doi: 10.1007/978-3-662-04223-6.

[102] J. Brookes, R. Bufacchi, J. Kondoh, D. M. Duffy, and R. A. McKendry, "Determining biosensing modes in SH-SAW device using 3D finite element analysis," *Sensors and Actuators, B: Chemical*, vol. 234, 2016, doi: 10.1016/j.snb.2016.03.103.

[103] M. J. Vellekoop, "Acoustic wave sensors. Theory, design and physicochemical applications," *Sensors and Actuators A: Physical*, vol. 63, no. 1, 1997, doi: 10.1016/s0924-4247(97)80433-5.

[104] D. W. Branch and S. M. Brozik, "Low-level detection of a Bacillus anthracis simulant using Love-wave biosensors on 36°YX LiTaO3," *Biosensors and Bioelectronics*, vol. 19, no. 8, 2004, doi: 10.1016/j.bios.2003.08.020.

[105] J. Xu, J. S. Thakur, F. Zhong, H. Ying, and G. W. Auner, "Propagation of a shear-horizontal surface acoustic mode in a periodically grooved AlN/Al 2O 3 microstructure," *Journal of Applied Physics*, vol. 96, no. 1, 2004, doi: 10.1063/1.1753660.

[106] N. F. Naumenko, "Application of exceptional wave theory to materials used in surface acoustic wave devices," *Journal of Applied Physics*, vol. 79, no. 12, 1996, doi: 10.1063/1.362624.

[107] E. Gizeli, C. R. Lowe, M. Liley, and H. Vogel, “Detection of supported lipid layers with the acoustic Love waveguide device: Application to biosensors,” *Sensors and Actuators, B: Chemical*, vol. 34, no. 1–3, 1996, doi: 10.1016/S0925-4005(96)01837-0.

[108] B. A. Martin, S. W. Wenzel, and R. M. White, “Viscosity and density sensing with ultrasonic plate waves,” *Sensors and Actuators: A. Physical*, vol. 22, no. 1–3, 1990, doi: 10.1016/0924-4247(89)80062-7.

[109] J. Kondoh, Y. Matsui, and S. Shiokawa, “New biosensor using shear horizontal surface acoustic wave device,” *Japanese Journal of Applied Physics*, vol. 32, no. 5S, 1993, doi: 10.1143/JJAP.32.2376.

[110] A. P. Campitelli, W. Wlodarski, and M. Hoummady, “Identification of natural spring water using shear horizontal SAW based sensors,” *Sensors and Actuators, B: Chemical*, vol. 49 B49, no. 3, 1998, doi: 10.1016/s0925-4005(98)00120-8.

[111] Y. Hur, J. Han, J. Seon, Y. E. Pak, and Y. Roh, “Development of an SH-SAW sensor for the detection of DNA hybridization,” *Sensors and Actuators, A: Physical*, vol. 120, no. 2, 2005, doi: 10.1016/j.sna.2005.01.027.

[112] Y. Q. Fu *et al.*, “Advances in piezoelectric thin films for acoustic biosensors, acoustofluidics and lab-on-chip applications,” *Progress in Materials Science*, vol. 89, pp. 31–91, 2017, doi: 10.1016/j.pmatsci.2017.04.006.

[113] M. Cole, G. Sehra, J. W. Gardner, and V. K. Varadan, “Development of smart tongue devices for measurement of liquid properties,” *IEEE Sensors Journal*, vol. 4, no. 5, 2004, doi: 10.1109/JSEN.2004.832855.

[114] H. Nishiyama, N. Saito, T. Yashima, K. Sato, and Y. Inoue, “Effect of shear horizontal leaky surface acoustic wave on selectivity for ethanol decomposition of a copper thin-film catalyst deposited on a positively polarized ferroelectric LiTaO3 single crystal,” *Surface Science*, vol. 427–428, 1999, doi: 10.1016/S0039-6028(99)00256-3.

[115] T. Palacios *et al.*, “Nanotechnology for SAW devices on AlN epilayers,” in *Materials Science and Engineering B: Solid-State Materials for Advanced Technology*, 2002, vol. 93, no. 1–3. doi: 10.1016/S0921-5107(02)00022-3.

[116] K. Tsubouchi and N. Mikoshiba, “ZERO TEMPERATURE COEFFICIENT SAW DELAY LINE ON AIN EPITAXIAL FILMS.,” in *Ultrasonics Symposium Proceedings*, 1983, vol. 1. doi: 10.1109/ultsym.1983.198063.

[117] C. Caliendo and P. Imperatori, “High-frequency, high-sensitivity acoustic sensor implemented on ALN/Si substrate,” *Applied Physics Letters*, vol. 83, no. 8, 2003, doi: 10.1063/1.1604482.

[118] K. Tsubouch and N. Mikoshiba, “Zero-Temperature-Coefficient SAW Devices on AlN Epitaxial Films,” *IEEE Transactions on Sonics and Ultrasonics*, vol. 32, no. 5, 1985, doi: 10.1109/T-SU.1985.31647.

[119] T. Shiosaki, Y. Mikamura, F. Takeda, and A. Kawabata, “HIGH-COUPLING AND HIGH-VELOCITY SAW USING ZNO AND ALN FILMS ON A GLASS SUBSTRATE.,” *IEEE Transactions on Ultrasonics, Ferroelectrics, and Frequency Control*, vol. UFFC-33, no. 3, 1986, doi: 10.1109/t-uffc.1986.26836.

[120] P. K. Kuo, G. W. Auner, and Z. L. Wu, “Microstructure and thermal conductivity of epitaxial AlN thin films,” *Thin Solid Films*, vol. 253, no. 1–2, 1994, doi: 10.1016/0040-6090(94)90324-7.

[121] L. G. Pearce, R. L. Gunshor, and R. F. Pierret, “Sputtered Aluminum Nitride on Silicon for SAW Device Applications,” 2008. doi: 10.1109/ultsym.1981.197647.

[122] S. Wu, L. Wu, J. H. Chang, and F. C. Chang, “SAW modes on ST-X quartz with an AlN layer,” *Materials Letters*, vol. 51, no. 4, 2001, doi: 10.1016/S0167-577X(01)00313-5.

[123] S. Wu, Y. C. Chen, and Y. S. Chang, “Characterization of AlN films on Y-128° LiNbO3 by surface acoustic wave measurement,” *Japanese Journal of Applied Physics, Part 1: Regular Papers and Short Notes and Review Papers*, vol. 41, no. 7 A, 2002, doi: 10.1143/jjap.41.4605.

[124] V. Mortet *et al.*, “Surface acoustic wave propagation in aluminum nitride-unpolished freestanding diamond structures,” *Applied Physics Letters*, vol. 81, no. 9, 2002, doi: 10.1063/1.1503875.

[125] J. Xu *et al.*, “Angular dependence of surface acoustic wave characteristics in AlN thin films on a-plane sapphire substrates,” *Applied Physics A: Materials Science and Processing*, vol. 83, no. 3, 2006, doi: 10.1007/s00339-006-3520-5.

[126] J. Xu, G. Hu, G. W. Auner, and H. Ying, “Mass sensitivity of dual mode SAW delay lines on AlN/sapphire structure,” *Electronics Letters*, vol. 41, no. 22, 2005, doi: 10.1049/el:20053193.

[127] X. Du, *Design and fabrication of a prototype aluminum nitride-based pressure sensor with finite element analysis and validation*. 2012. [Online]. Available: https://search.proquest.com/openview/b3d561167d3c4446be6a4d0610cb9a42/1?pq-origsite=gscholar&cbl=18750

[128] G. Hu, *Acoustic wave sensing system based on aluminum nitride dual-mode sensors and digital phase detection approach*. 2008. [Online]. Available: https://search.proquest.com/openview/9f707bd496af1ab5c52323810e07cf14/1?pq-origsite=gscholar&cbl=18750&casa_token=eK1Ye6u1I_QAAAAA:zBjwswuyXrlcPV-On_ZhZ1bDGrEWeKRZkw-0m4shtP9rm6va-WbOv6pksEgajVg_VLUWDDz1

[129] K. Nakamura, *Ultrasonic transducers: Materials and design for sensors, actuators and medical applications*. 2012. doi: 10.1533/9780857096302.